Annales Societatis Geologorum Poloniae (2024), vol. 94: 83–110 https://doi.org/10.14241/asgp.2024.02

INTEGRATED SUBSURFACE CHARACTERISATION OF THE RÖT SUCCESSION OF THE BOLESŁAWIEC SYNCLINE (SW POLAND): STRATIGRAPHIC AND TECTONIC CONSTRAINTS OF THE GEOLOGICAL RECORD

Karol DURKOWSKI [1, 2] *, Krzysztof MASTALERZ [3] & Anna FIJAŁKOWSKA-MADER [4]

[1] *KGHM Cuprum Research & Development Centre, gen. Wł. Sikorskiego 2–8, 53-659 Wrocław, Poland; e-mail: karol.durkowski@kghmcuprum.com*
[2] *AGH University of Science and Technology, Faculty of Geology, Geophysics, and Environmental Protection, Mickiewicza 30, 30-059 Kraków, Poland*
[3] *2005 Bow Drive Coquitlam, Brit. Col. V3E 1X4, BC, Canada; e-mail: krzys_mastalerz@yahoo.com*
[4] *Polish Geological Institute - National Research Institute, Holy Cross Branch, Zgoda 21, PL-25-953 Kielce, Poland; e-mail: amad@pgi.gov.pl*
** Corresponding author*

Durkowski, K., Mastalerz, K. & Fijalkowska-Mader, A., 2024. Integrated subsurface characterisation of the Röt succession of the Bolesławiec Syncline (SW Poland): stratigraphic and tectonic constraints of the geological record. *Annales Societatis Geologorum Poloniae*, 94: 83–110.

Abstract: This study presents the first comprehensive geological analysis of the Triassic Röt sedimentary succession in the Bolesławiec Syncline (BS), North-Sudetic Synclinorium (NSS), SW Poland, and fills information gaps regarding the local lithology, stratigraphy, extent and organisation of this succession. During Triassic time, the BS was located on the southern periphery of the epicontinental Germanic (Central European) Basin. The mixed siliciclastic-carbonate Röt succession transgressively overlies the continental siliciclastics of the Buntsandstein (Bunter), locally with the occurrence of a stratigraphic gap. The Röt succession displays a complex vertical organisation with basic, about 1-m-scale, fine siliciclastic-carbonate couplets, and larger-scale sequences. The well-log profiles allow identification and provisional subdivision of the succession into several 1D sequences, 10–25 m thick, which can be correlated across the study area. The collected palynological material indicated the latest Olenekian to early Anisian age of the local Röt succession. A surprisingly strong thickness diversification of the succession, as well as its frequent incompleteness, evidenced by both palynology and correlation of well-log profiles, is interpreted in terms of local erosion, non-deposition, synsedimentary tectonic activity, and later tectonic deformation. The authors conclude that synsedimentary tectonics resulted in faulting of the area and was the principal factor responsible for differential subsidence and variable sediment accumulation rates. The lower stratigraphic interval of the Röt succession is defined explicitly by the presence of numerous and diversified small-scale soft-sediment deformational structures. The coincidental occurrence of the first marine deposits in the BS area, together with the intense soft-sediment deformation appear to indicate that the end of Early Triassic transgression was associated with intensified regional seismic/tectonic activity. The Röt sedimentary succession of the BS area also was affected by younger tectonic deformation. The pre-Cenomanian events brought about at least local uplift and limited erosion of the Röt succession. Late Cretaceous–Palaeogene inversion was responsible for the final development of the present-day structure of the NSS.

Key words: North-Sudetic Synclinorium, Germanic Basin, small-scale deformational structures, synsedimentary tectonics, palynology, basin architecture, sequence organisation.

Manuscript received 25 March 2023, accepted 10 November 2023

INTRODUCTION

The Röt succession of the North-Sudetic Synclinorium (NSS), SW Poland, represents the marginal-marine facies of the Germanic Basin, adjacent to the Bohemian-Vindelician Massif (Fig. 1). Such marginal-marine settings are relatively poorly known from the Germanic Basin because of the limited outcrops, especially in Poland, where most of the Triassic marine rocks are overlain by younger formations. The Röt strata of the NSS previously were described in terms of

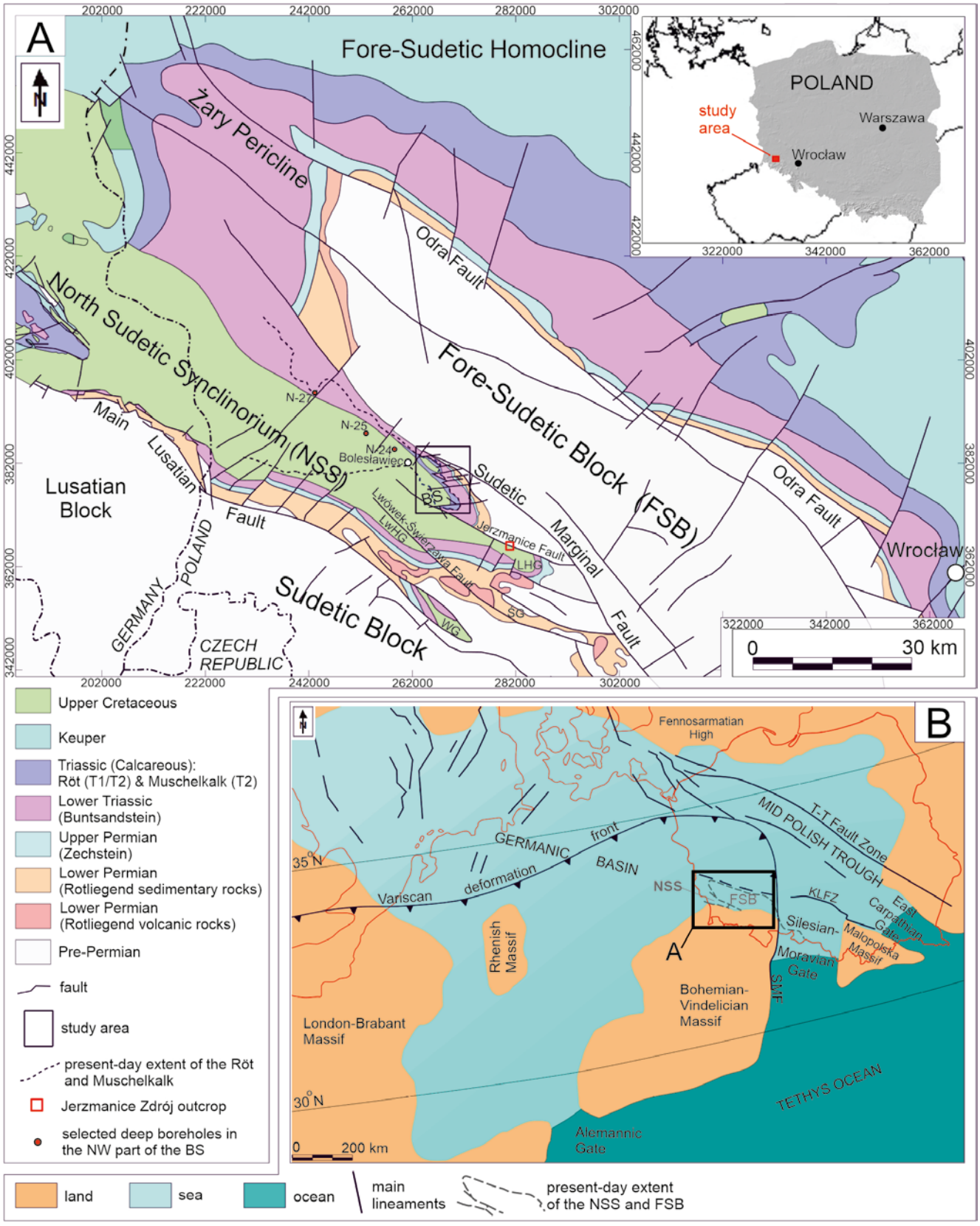

Fig. 1. Location of the study area. **A.** Simplified geological map without Cenozoic overburden of the North Sudetic Synclinoriun and adjoining areas (modified after Dadlez *et al.*, 2000; Hielscher and Hartsch, 2010 and Durkowski, 2022). Abbreviations: BS – Bolesławiec Syncline; ŚG – Świerzawa Graben; LHG – Leszczyna Half-Graben; LwHG – Lwówek Śląski Half-Graben; WG – Wleń Graben. **B.** Simplified palaeogeography of the Germanic Basin in the Middle Triassic (modified after Ziegler, 1982; Matysik and Szulc, 2019; Durkowski, 2022). Abbreviations: KLFZ – Kraków-Lubliniec (Hamburg) Fault Zone; T-T Fault Zone – Teisseyre-Tornquist Fault Zone; SMF – Silesian-Moravian Fault; N - Triassic palaeolatitudes; NSS – North Sudetic Synclinorium; FSB – Fore-Sudetic Block.

lithology and lithostratigraphy by several authors, but those studies were based on limited data (e.g., Noetling, 1880; Leśniak, 1973, 1978, 1979; Chrząstek, 2002).

This study presents the first comprehensive description and analysis of the Röt succession in the easternmost part of the NSS, the Bolesławiec Syncline (BS; Fig. 1A). The documentary material discussed here comes from cored intervals and corresponding geophysical wireline logs from several recently completed boreholes and is supported by palynological dating. One of the most striking observations concerns the abundance of diversified, small-scale, soft-sediment deformational structures within the Röt rocks (Durkowski, 2022). These rocks overlie a thick sandstone-siltstone succession of the local Buntsandstein facies, which is completely without similar deformational structures. Likewise, the overlying lower Muschelkalk carbonate rocks do not display small-scale soft-sediment deformation.

The study provides some new lines of evidence for more precise, regional correlations with corresponding rocks of other Germanic Basin peripheries (e.g., Małopolska-Silesia and Holy Cross Mountains), as well as centre-of-the-basin realms, such as the Fore-Sudetic Homocline, Polish-Danish Trough and Lower Saxony Basin. The comprehensive approach of this study also resulted in elucidating some impacts of younger tectonic events on the Röt geological record.

GEOLOGICAL SETTING

The Early-to-Middle Triassic configuration of the southern periphery of the Germanic Basin was quite diversified. The main area of this epicontinental basin was separated from the southerly Tethys Ocean by a strip of land, which included a few significantly elevated massifs and some narrow lowland areas (Fig. 1B). The elevated areas included the Vindelician-Bohemian and Małopolska Massifs, both of which remained emerged throughout the Triassic sedimentation period. The lowland areas ("the gates"), in turn, became periodically submerged, providing connections to the Tethys Ocean, and allowed transgressions of oceanic waters into the Germanic Basin (Szulc, 2000; Feist-Burkhardt *et al*., 2008; Matysik and Szulc, 2019).

The BS and the entire NSS, SW Poland (Fig. 1A) represent part of the late Variscan European foreland basin (Mazur *et al.*, 2010) and started accumulating sediments in the late Carboniferous (Milewicz, 1962, 1968; Sokołowski, 1967; Wojewoda and Mastalerz, 1989; Raczyński *et al.*, 1998; Śliwiński *et al.*, 2003; Solecki, 2011). During the early Permian, some of the NSS structural compartments took the form of narrow WNW–SSE-elongated grabens and/or half-grabens, which gathered diversified suites of continental sediments and volcanogenic rocks. The sediments reflected a strong response to synsedimentary tectonics and resulted in steep facies gradients, expressed as abrupt transitions between alluvial fan and lacustrine facies (Ostromęcki, 1973; Mastalerz, 1987, 1990; Wojewoda and Mastalerz, 1989).

The late Permian Period brought about restricted marine conditions in the NSS area, which was located along the southern, peripheral part of the large-scale Central European Zechstein Basin (Milewicz, 1976; Wojewoda and Mastalerz, 1989; Raczyński *et al.*, 1998; Mazur *et al.*, 2010; Chrząstek and Wojewoda, 2011).

During Triassic time, the NSS area still was located at the southern periphery of the eastern segment of the Central European Basin, commonly referred to as the Germanic Basin, with regard to its Triassic succession (Fig. 1B). The Early Triassic succession is dominated by widespread, continental sandstone and subordinate finer-grained siliciclastics, defined as the Radłówka Formation by Milewicz (1985) and typical of the Germanic Buntsandstein facies (Sokołowski, 1967; Szyperko-Teller, 1997; Dadlez *et al.*, 1998; Bachmann *et al.*, 2010). The marine transgression, which reached the NSS area by the end of the Early Triassic, led to deposition of interbedded carbonate, commonly marly, and fine-grained siliciclastics of the Röt facies. A progressing transgression in the Middle Triassic resulted in deposition of carbonates, termed the Muschelkalk. This change from siliciclastic-dominated Buntsandstein facies into the ones, dominated by sulphate-bearing Röt and Muschelkalk carbonates, reflects the transition from fully continental conditions during the Early Triassic to brackish and then fully marine ones later during the Middle Triassic. Distinct cyclic organisation and associated fossils allowed establishment of relatively long-distance correlation and biostratigraphic subdivision of the open-marine Muschelkalk carbonates (e.g., Dadlez, 1998; Dadlez *et al.*, 1998; Bachmann *et al.*, 2010). However, the stratigraphy of the basin's peripheral areas is commonly ambiguous, owing to the scarcity of index fossils (Noetling, 1880; Scupin, 1902, 1913, 1932; Assmann, 1944; Kłapciński, 1959; Gajewska, 1964; Milewicz, 1962, 1985; Chrząstek, 2002; Śliwiński *et al.*, 2003). So far, both stratigraphic boundaries of the Röt succession have never been defined satisfactorily for establishment of a formal lithostratigraphic unit in the NSS area (e.g., Chrząstek, 2002).

MATERIAL AND METHODS

This study is based on extensive data, provided by 20 boreholes completed between 2011 and 2016 in the BS area (Fig. 2). The carbonate Triassic succession (the Röt and Muschelkalk facies) was investigated by 14 boreholes, including six fully cored, and two partially cored wells (Figs 2–4). Limited field observations and measurements were collected by the authors in two quarries, situated in Raciborowice ("Podgrodzie") and Jerzmanice Zdrój (Figs 1A, 2). These newly acquired sets of borehole and field data were complemented by documentary materials on 32 older boreholes, completed earlier (1970's) in the study area, and by a report on the "Podgrodzie" limestone quarry (Drozdowski *et al.*, 1978). All the cored intervals of the Triassic carbonate succession have been macroscopically described with an emphasis on the lithology and structural/textural features. A calcimetric analysis was used to determine the content of the carbonate minerals (calcite and dolomite) in the rock formation.

A set of modern geophysical wireline logs was recorded by Geofizyka Kraków in all 20 boreholes, completed in

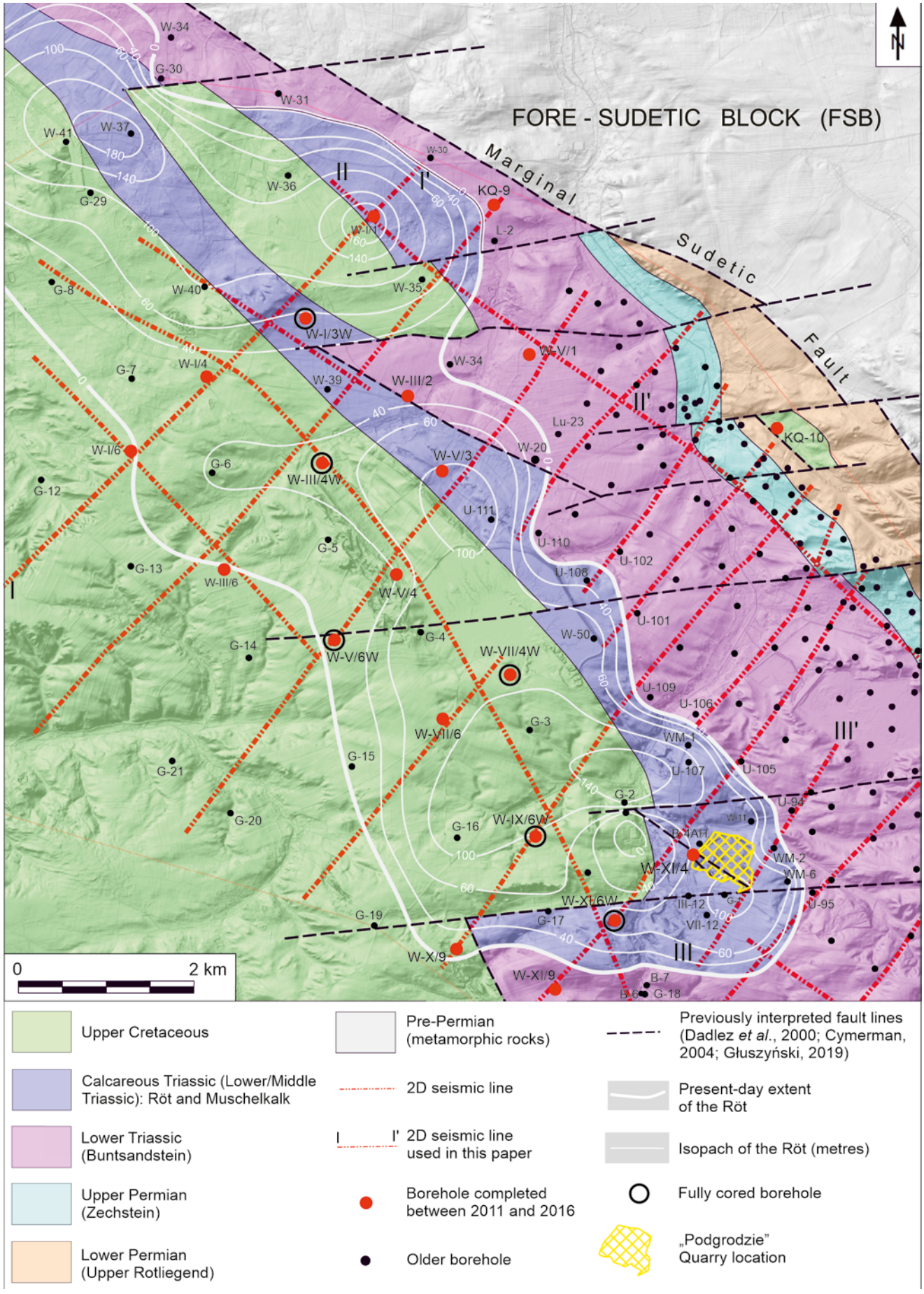

Fig. 2. Background geological map of the study area (without Cenozoic overburden), modified from Dadlez *et al*. (2000; see also Durkowski, 2022) with an overlay of the isopach (white contours) map of the Röt succession.

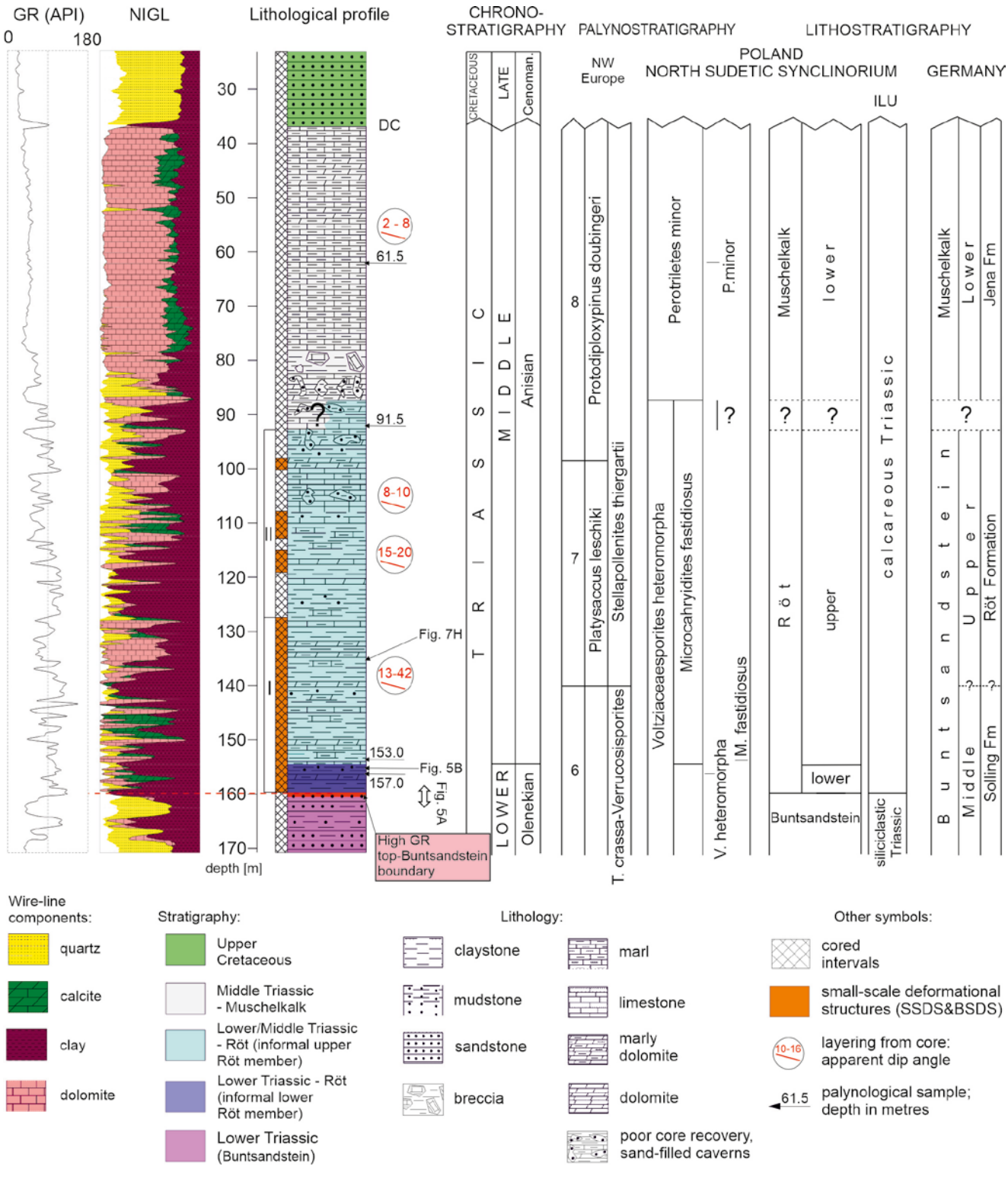

Fig. 3. Generalized lithostratigraphic column of the Röt and Muschelkalk - borehole W-XI/6W.
Abbreviations: GR – Gamma Ray log; NIGL – numerical interpretation of the results of geophysical logs; ILU – informal lithostratigraphic units; DC – disconformity; I and II – first (main) and second deformation horizons; (Chronostratigraphy after Cohen *et al*., 2013; SW Poland lithostratigraphy after Chrząstek, 2002; Śliwiński *et al*., 2003; Petrovic and Aigner, 2017; German lithostratigraphy after Bachmann *et al*., 2010; Menning and Hendrich, 2017; Palynostratigraphy after Orłowska-Zwolińska, 1984, 1985; Heunisch, 1999; Kürschner and Herngreen, 2010).

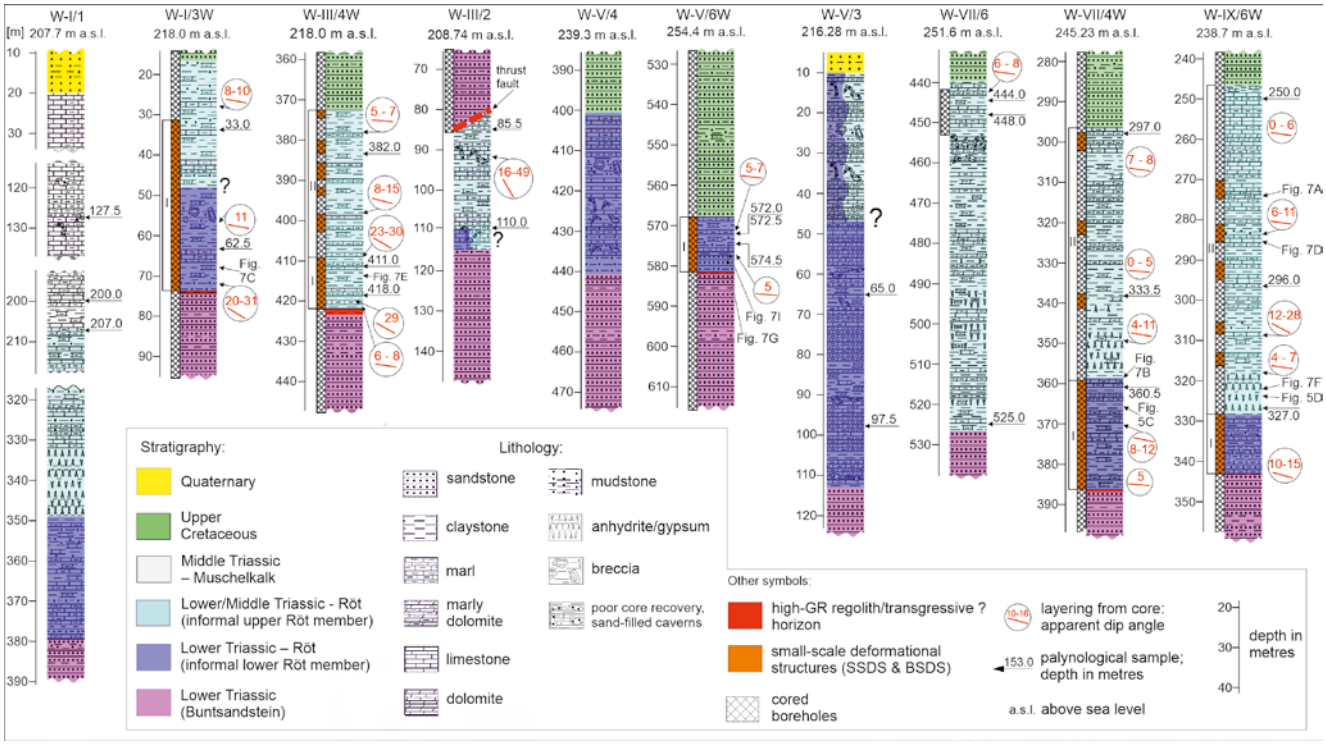

Fig. 4. Selected borehole sections of the Röt in the Bolesławiec Syncline (note locations of palynological samples and attitude of stratification to the core axis; all boreholes are vertical; for borehole locations see Figures 2 and 12).

2011–2016. These wireline logs provided data for a simplified composition analysis, based on the calculated contents of the standard wireline minerals/lithologies (clay, quartz, carbonate and sulphate) and for analysis of the vertical sequence (Fig. 3). The results of the numerical "Interlog" lithological evaluation of the rock formation, based on the wireline logs, were also available to the authors (Ratajczyk *et al.*, 2015; Fig. 3).

Selected 2D seismic-reflection data aided in interpretation of the subsurface structure, stratigraphy and lithostratigraphic relationships of the study area (Fig. 2). The seismic data were acquired, processed, and originally interpreted by Geopartner Sp. z o.o. (Miluk *et al.*, 2016). The survey lines were re-interpreted and converted to the depth domain by Głuszyński *et al.* (2019). Three of these seismic cross-sections, which total about 17 km in length, are presented in this article. The maps of the top of the siliciclastic Buntsandstein and isopachs of the Röt succession were constructed using the borehole data with the support of the seismic results.

The spore-pollen analysis was performed on 31 rock samples, collected from 10 boreholes and two outcrops (Appendix). The samples were treated with the HCl and HF, according to the method described in Orłowska-Zwolińska (1983). The residues were sieved through a 10 μm nylon mesh and placed in glycerine-gel microscope thin sections. A hundred palynomorphs per slide were counted, using the Leitz Laborlux microscope. Wherever samples contained less palynomorphs, all forms were included in the analysis.

RESULTS AND BASIC INTERPRETATION

Lithology

There are almost no outcrops of the Röt succession in the BS area; only its uppermost fragment, where the contact with the Muschelkalk facies is exposed on a limited scale in a quarry, near Raciborowice (Figs 2, 5). Thus, the borehole documentation, especially cores and wireline logs, was elaborated for lithological characterisation of the succession.

The Röt succession in the study area represents a mixed siliciclastic-carbonate depositional system and consists mainly of calcareous mudstone, marl, marly limestone and dolostone, with less frequent and thinner intercalations of poorly sorted, fine-grained siliciclastics and "cleaner" carbonate rocks (Tab. 1; Figs 3, 4, 6). The Röt rocks overlie the monotonous sandstone-dominated Buntsandstein facies (Fig. 6A) and are locally overlain by a limestone-dolostone-dominated Muschelkalk facies (Figs 3, 4). Sulphate, both gypsum and anhydrite, and sulphate cementation zones were encountered only locally, in a few boreholes. The most important features of the lithological variability of the Röt succession are summarized in Table 1.

The lowermost part of the Röt succession contains larger amounts of fine siliciclastic rocks than its middle and upper parts, which are, in turn, enriched in carbonate rocks. However, a subdivision of this succession into smaller-scale lithostratigraphic members would be difficult on the basis of standard field/core criteria, owing to the lack of strong and consistent lithological differentiation. It is different,

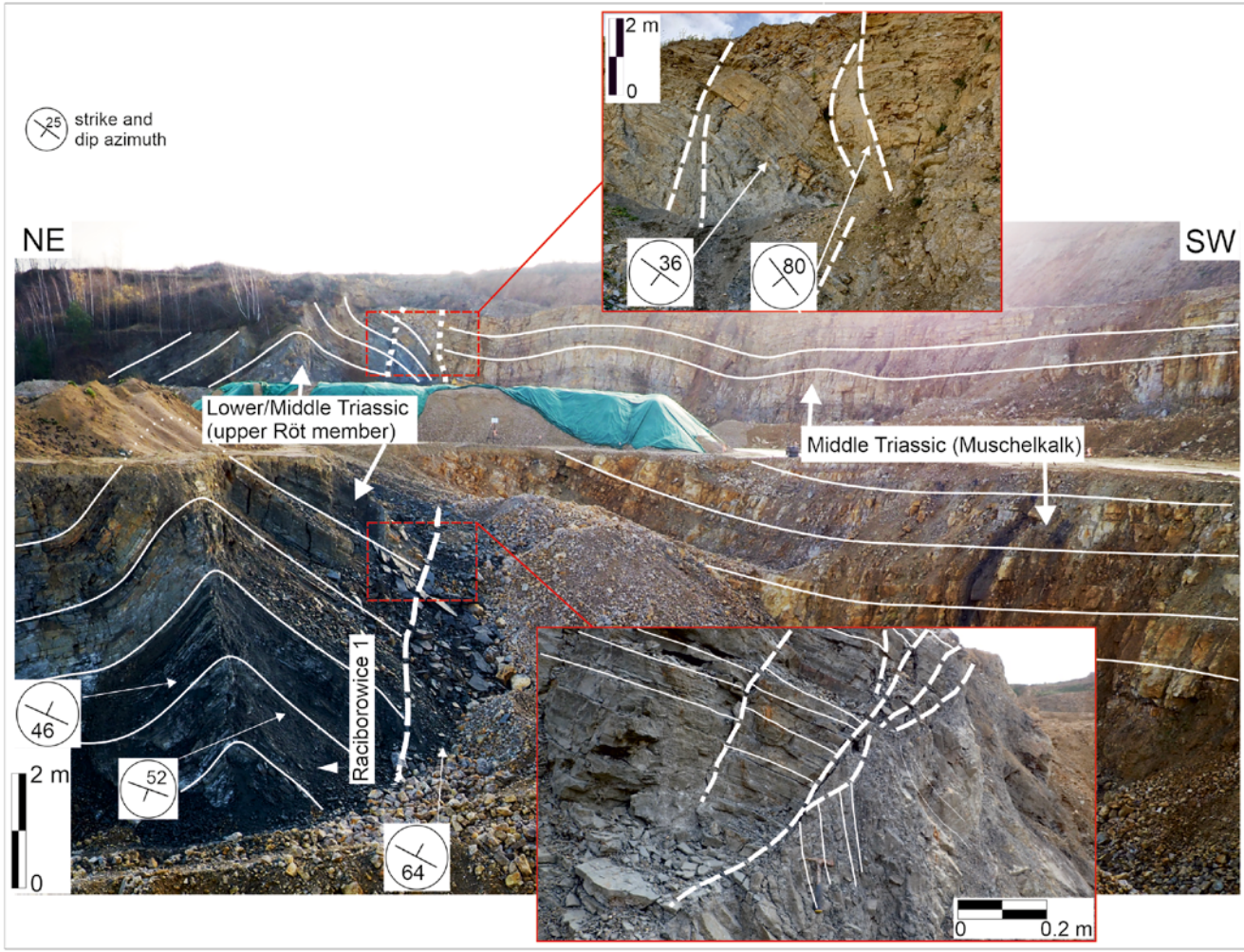

Fig. 5. Selected photographs of the southern part (looking southeastwards) of the "Podgrodzie" Quarry in Raciborowice, which depict deformation style of the upper Röt member (lower left-side corner) and Muschelkalk succession; insets illustrate two details of fault zones, observed along the lower and upper levels of the quarry. Abbreviations: Raciborowice 1 – location of palynological sample.

however, where sulphates occur in a particular borehole succession. In such instances, the base of the first significant sulphate interval (Figs 4, 7, 8) appears to mark the upper boundary of the lowermost, fine-siliciclastic-dominated member. Such a potential subdivision would be very similar to the one, proposed by Tokarski (1965) for the Röt succession of the Fore-Sudetic Homocline, farther north.

The new, completely cored boreholes provided abundant evidence of small-scale deformational structures in the Röt succession (Figs 3, 4, 6, 9; see also Durkowski, 2022). These deformational structures belong to two distinct groups: 1) brittle-style deformational structures and 2) soft-sediment deformational structures. The brittle-style deformational structures include small-scale, irregular pockets of sedimentary breccia, core-scale inverse and normal faults, and neptunian and injection dykes. (Figs 6, 9). Small-scale, fold-style deformations occur locally along fault terminations (Figs 6B, 9I). Injection dykes occur commonly and have been observed in all of the new boreholes (Durkowski, 2022). They are accompanied locally by intraformational breccias (e.g., Fig. 9B–C, I). The neptunian dykes are far less common and have only been observed in a few instances (e.g., Fig. 9H). The most prominent occurrence of sediment liquefaction structures was encountered within the lowermost part of this succession in borehole W-V/6W. Numerous other structures (e.g., load casts, ball-and pillow, flame structures, convolute lamination), related to unstable/reverse sediment density stratification (*sensu* Dżułyński 1966; Anketell *et al.*, 1970; see also Gradziński *et al.*, 1986), occur scattered throughout the Röt intersections in the cored boreholes (e.g., Fig. 9A, B, G, H, I; see also Durkowski, 2022).

Both types of small-scale deformational structures commonly occur within the same stratigraphic intervals of the Röt (Figs 3, 4). The thicknesses of the intervals, which host deformational structures vary from single occurrences to about 30–40 m of almost continuous zones of variable deformations, as in boreholes W-I/3W and W-XI/6W (Figs 3, 4). It is important to note that in the lower parts of the Röt succession, the small-scale sediment deformational structures occur more commonly and constitute thicker intervals, almost consistently across the entire study area ("main deformed interval" of Durkowski, 2022; Figs 3, 4).

Table 1

Features of the lithological variability of the Röt succession.

Lithological groups	Lithology	Common occurrence	Strata/package thickness [m]	Features/general characteristics	Sedimentary structures, texture and grain type
Siliciclastics	Claystone, mudstone, (siltstone, breccia)	Lower Röt, progressively less common up the succession	<0.01– ~1.0	Grey, dark grey to black; poorly to moderately sorted; common gradational contacts; commonly interbedded with carbonate and mixed-composition packages	Planar and wavy parallel, rarely ripple-cross lamination; small-scale graded bedding, homogenous-massive, load casts and sole structures, slump folds, (chaotic – intraformational breccia), small-scale erosional structures, SSDS and BDSD; gradational texture changes (e.g., grain size) within packages; (bioturbation structures, burrows)
Mixed composition	Marl, marly limestone, calcareous mudstone	Entire Röt		Grey to light grey, beige; poorly sorted; commonly interbedded with siliciclastic and carbonate packages	Wavy, wispy, flaser and parallel lamination; small-scale graded bedding; locally siliciclastic intraclasts and mudstone chips; bioturbation structures, burrows; SSDS and BDSD
Carbonate	Limestone, dolostone	Mostly middle and upper Röt	<0.01– ~0.5; to ~1.5 in upper Röt member[1]	Light grey to grey and beige; usually sharp lower boundaries and frequently transitional upper; commonly interbedded with mixed composition and siliciclastic packages	Lime mudstone, wackestone, grainstone, packstone, bioclastic limestone, intraclasts; wavy, wispy, flaser, parallel and ripple cross -lamination, BDSD and SSDS; small- to medium-scale, low-angle cross-stratification; bioturbation structures, burrows, coquina layers; cryptalgal laminations, mud/syneresis cracks, firmground/ hardground, micritization
Sulphates	Gypsum, anhydrite	Mostly middle Röt; (Figs 3, 4 and 12)	~2.0– ~16.0	Light grey to grey, orange; translucent; usually interbedded with thin packages of carbonates, sharp boundaries between sulphates and carbonates; cracks in carbonates filled with gypsum	Banded parallel bedding and lamination; cryptalgal laminations, syneresis cracks, rarely small-scale, fold-style deformations

Abbreviations: SSDS – soft-sediment deformational structures; BDSD – the brittle-style deformational structures.

Vertical organisation

The mixed siliciclastic-carbonate succession of the Röt displays distinct, though complex, vertical succession of strata in the BS area. The repetitive couplets of contrasting composition (lithology) range from millimetres to metres thick. The simple, lamination-to-centimetre-scale repetitions occur very commonly throughout the succession and include the fine-grained siliciclastics, carbonates and sulphates (Fig. 6B, C, D). However, complex patterns of oscillatory, fine-siliciclastic and carbonate repetitions (couplets) also occur commonly on scales of tens of centimetres to a few metres (Fig. 6B, D). The tops of the carbonate units within such couplets are usually sharp, while the siliciclastic-carbonate contacts are gradual. Such thicker-scale oscillations can be easily identified on some geophysical wireline logs. The GR (natural gamma radiation), and RHOB (formation density), are the most reliable logs for simplified lithological evaluation (cf. Schlumberger, 1974; Asquith and Gibson, 1982). The GR response usually corresponds directly to the amount of clay minerals and organic matter in the rock formation. The elevated RHOB responses are related to increased carbonate content, especially dolomite, but also anhydrite. Clay-rich lithologies and gypsum usually display low RHOB densities. The mixed-composition lithologies (e.g., marl, calcareous mudstone, poorly sorted, matrix-rich sandstones) require some additional logs (e.g., neutron porosity, density porosity, resistivity, sonic, etc.) for reliable lithological evaluation (cf. Schlumberger, 1974; Asquith and Gibson, 1982).

Both, density (RHOB) and natural gamma (GR) logs display high-frequency oscillatory variation in boreholes penetrating the Röt succession (Fig. 7). These basic oscillations correspond to intervals of contrasting lithology in the order of approximately 1 m in thickness (Fig. 6B, D). Such basic oscillations are organized into 3- to 8-m-thick asymmetric patterns (Fig. 7), which usually display overall, upward-increasing trends in rock density and corresponding

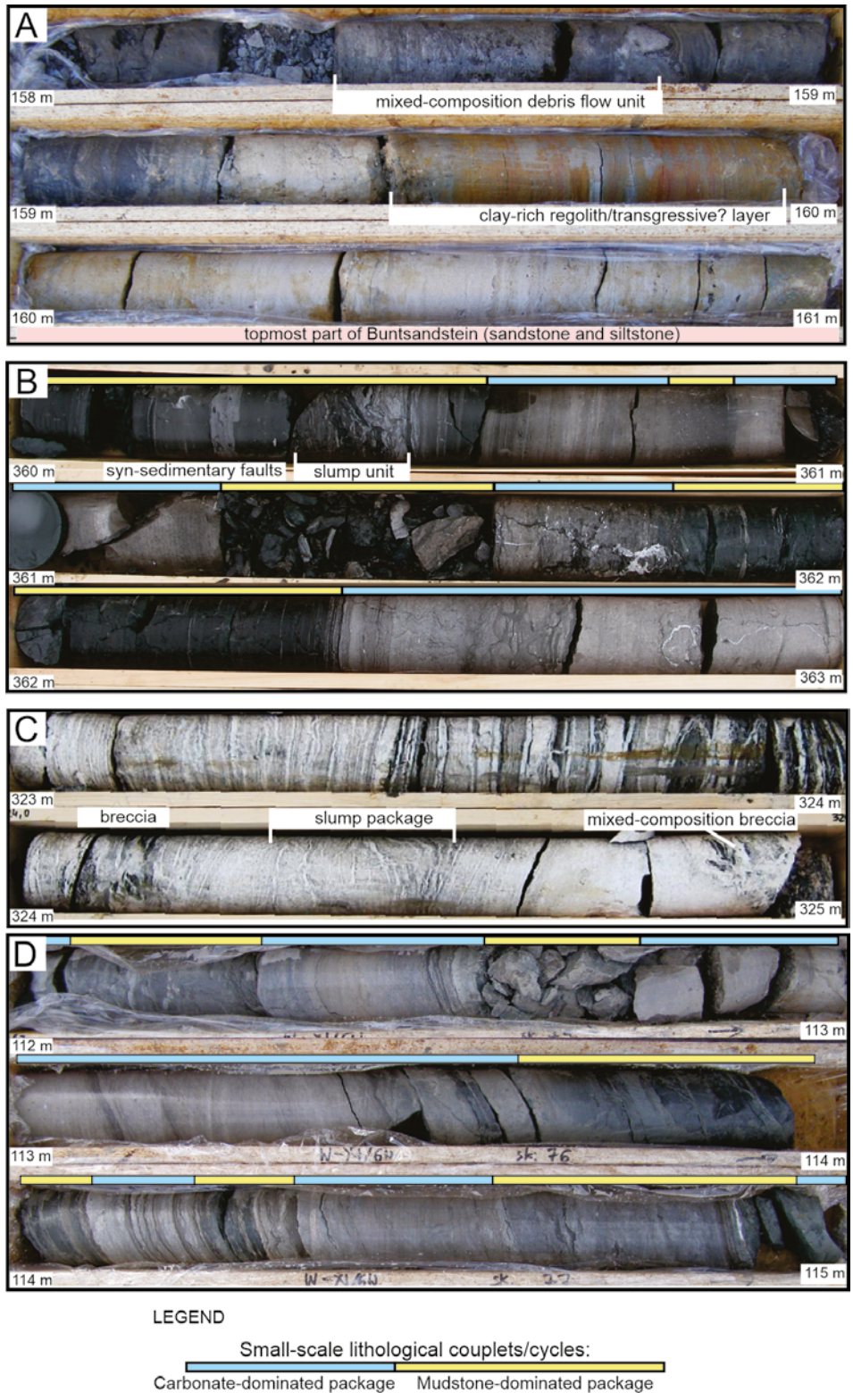

Fig. 6. Selected examples of the Röt lithologies in the Bolesławiec Syncline (depths indicated) **A.** Contact of the Buntsandstein (pale grey, crudely stratified sandstone to thick laminated siltstone) with Röt (pale to dark grey, strongly brecciated, calcareous mudstone and minor limestone) in borehole W-XI/6W (depth 158–161 m); note the rusty, clay-rich regolith-like or transgressive layer at the contact. **B.** Moderately thick interbedded packages of dark-grey mudstone and lighter marly calcarenites (basic oscillatory couplets) of the lower Röt in borehole W-VII/4W (depth 360–363 m); note the contorted, slump-related, carbonate-rich unit within the uppermost mud-rich package. **C.** Interbedded gypsiferous siltstone and laminated marly limestone with secondary satin sparry gypsum, filling sub-horizontal fractures of the middle Röt in borehole W-IX/6W (depth 323–325 m); note the contorted, slump-related package (lower box) and layers of mixed-composition breccia in the lower part of the box. **D.** Interbedded, thin-to-thick laminated and thin-to-medium bedded, light grey dolomitic limestone and darker marly mudstone and shale of the upper Röt in borehole W-XI-6W (depth 112–116 m); the noticeable oscillatory pattern involves thicker, lime-rich and thinner, mud-rich packages (basic oscillatory couplets).

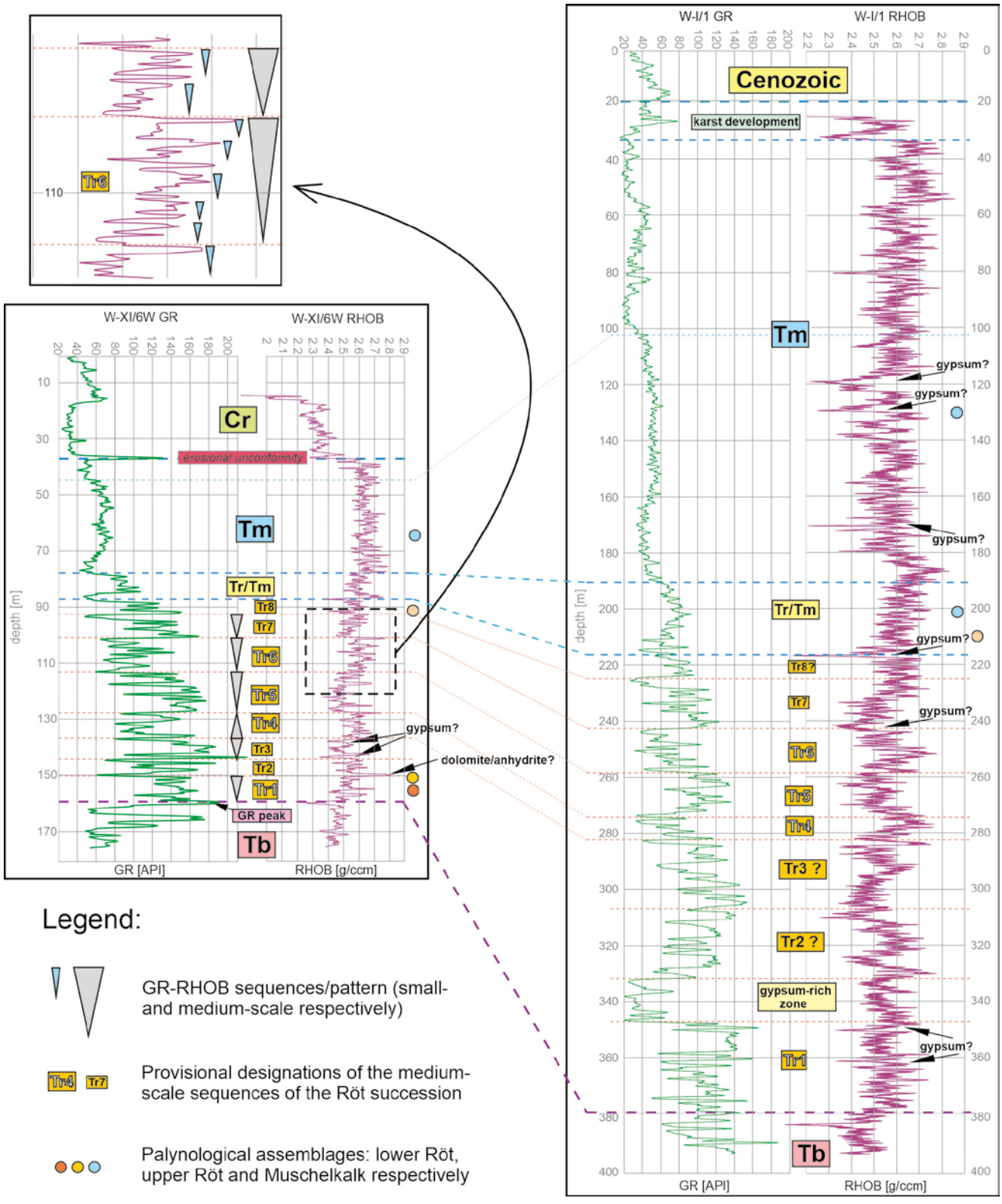

Fig. 7. Sequence structure of the Röt of the Bolesławiec Syncline, illustrated by variability of the GR (natural gamma) and RHOB (formation density) wireline logs; examples from boreholes W-XI/6W and W-I/1 demonstrate provisional subdivision of the Röt into informal small-scale lithostratigraphic end-members and their tentative correlation.

upward-decreasing GR trends. These wireline features correspond to upwards-cleaning (progressively less clay) strata sequences, which are typified by clay-rich (mudstone) bases and sharp carbonate-rich tops. These patterns are provisionally identified here as small-scale strata sequences (Fig. 7).

The higher-order, complex strata sequences include approximately 10- to 25-m-thick intervals, which enclose some small-scale patterns. These latter intervals are characterised by variable tendencies (upwards-increasing, upwards-decreasing and semi-symmetric patterns of RHOB

and GR), which correspond to longer-term, gradual trends of lithological change and are terminated by distinct, abrupt breaks. These trends are designated here as medium-scale strata sequences (Fig. 7).

The complete Röt succession includes several medium-scale strata sequences, as illustrated in Figure 7. The pattern of the medium-scale GR-RHOB patterns, encountered in the W-XI-6W borehole record, is tentatively regarded as the one representative of the local complete Röt succession and designated the "standard Röt GR-RHOB pattern" (Fig. 7). The repetitive nature of specific strata sequences within this formation in different boreholes appears to indicate that the well-log signatures can be used for a consistent subdivision of the Röt succession and for the correlation of such subdivisions, at least across the entire study area (Fig. 7).

The GR-RHOB-defined medium-scale Röt sequences differ in the individual boreholes with regard to their thicknesses. Such differences appear to be quite significant; some of the sequences identified in borehole W-I/1 are about twice as thick as their counterparts in borehole W-XI/6W (Fig. 7). Consequently, the entire Röt succession in W-I/1 appears to be complete (?) and is approximately twice as thick as that in borehole W-XI/6W. It is worth noting that some sequences of the standard Röt pattern appear to be missing in the other boreholes (Fig. 8).

Stratigraphic boundaries and extent of the Röt succession

Near the base of the first carbonate-rich package, there is a characteristic clay-rich, rusty-coloured layer, which overlies the light-grey, poorly sorted and moderately cemented Buntsandstein silty sandstone (Fig. 6A). This layer is tentatively interpreted by the authors as representing either a regolith-like horizon, which had developed over an abandoned and weathered surface of the topmost Buntsandstein succession, or a package of transgressive, fine-grained sediment (Figs 3, 4). The wireline logs allowed the identification of a high natural gamma-ray (GR) peak, which corresponds to this rusty, clay-rich layer (Figs 3, 4, 7) in most boreholes. The authors propose considering this layer, which occurs in most wells, as the lower boundary of the Röt succession in the BS area (Fig. 7).

Severe potential controversies appear, when one tries to distinguish the Röt and Muschelkalk successions, both of which include common-to-predominant carbonate rocks in the study area. The scarcity of index fossils makes this a difficult task. The Röt traditionally has been described as a mixed in composition, a carbonate-fine siliciclastic succession, while the Muschelkalk facies are known to be completely dominated by carbonate rocks (Figs 3, 4; cf. Scupin, 1902, 1913, 1932; Watycha, 1951; Milewicz, 1985; Chrząstek 2002). The authors decided to follow this lithological change, which is well expressed in wireline logs as an increase in rock density (RHOB) and monotonous character of the GR curve, in placing a provisional boundary between these two successions (Fig. 7). Palynological data, collected during this study (Figs 3, 4, 7, 8; Tab. 2), appear to support the aforementioned wireline/lithological criteria.

The Röt and Muschelkalk successions of the study area usually are overlain by significantly younger (Late Cretaceous or Tertiary) rocks, distinct in terms of facies.

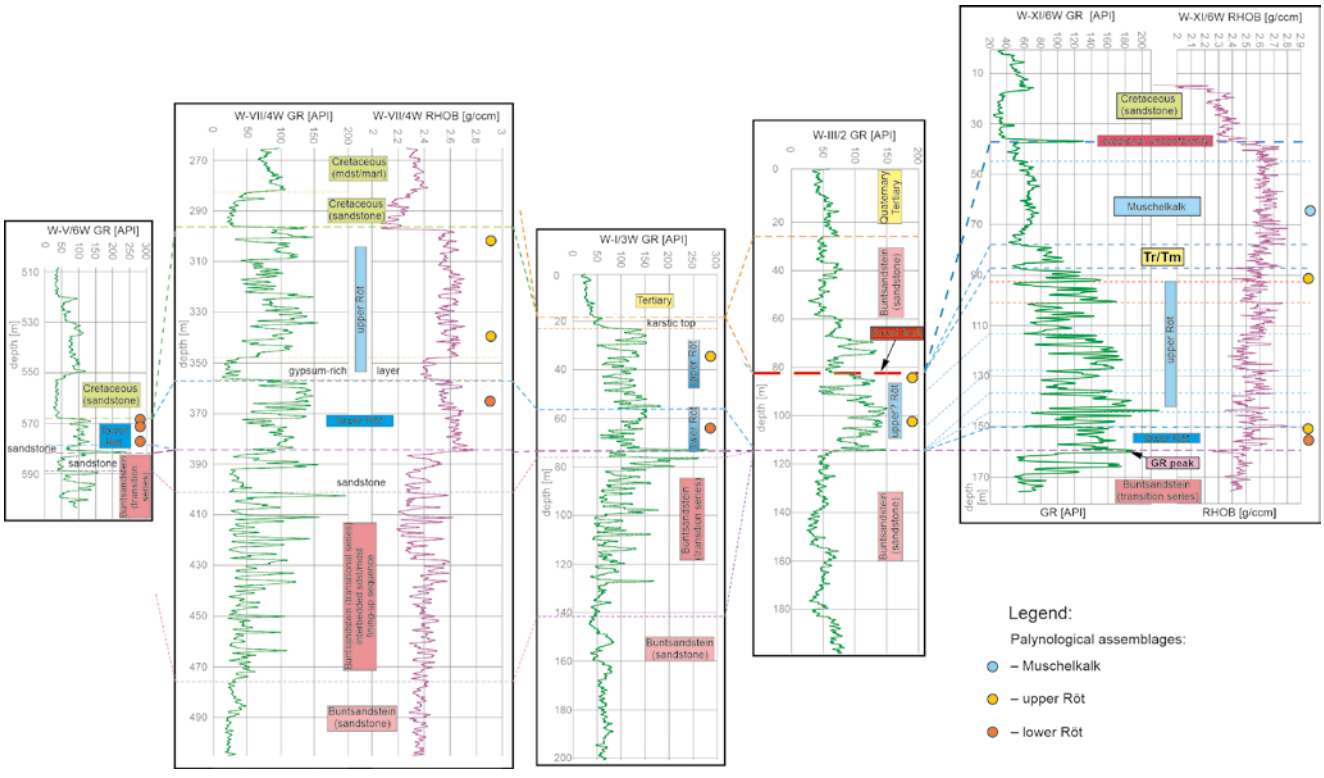

Fig. 8. Comparison of GR (natural gamma) well logs from boreholes W-V/6W, W-VII4W, W-I/3W and W-III/2 with the proposed correlation of principal and provisional smaller-scale lithostratigraphic units. The RHOB (formation density) logs (boreholes W-VII/4W and W-XI/6W) are added for better illustration of lithological variability.

Table 2

Characteristics of damaged (redeposited) (?) palynomorphs in the analyzed samples.

Nr	Borehole/ Outcrop	Depth [m]	Lithostratigraphic position	Palynostratigraphy	Proportion of damaged, redeposited and reworked palynomorphs [%]
1	W-I/1	127.5	Muschelkalk	*P. minor*?	50 (R + M)
2		200.0			40: 39 (R + M), 1 (B)
3		207.0	upper Röt member	*M. fastidious*	>1 (B, P?)
4	W-I/3W	33.0	upper Röt member	*M. fastidiosus*	0
5		62.5	lower Röt member	*V. heteromorphus*	50: 49 (R), 1 (B), >0,5 (Z?)
6	W-III/2	85.5	upper Röt member	barren sample	no data
7		110.0		*M. fastidious*	>1 (Z)
8	W-III/4W	382.0	upper Röt member	*M. fastidiosus*	1 (B)
9		411.0			1 (R)
10		418.0			1 (B)
11	W-V/3	65.0	lower Röt member	*V. heteromorphus*	50 (R)
12		97.5			30 (R)
13	W-V/6W	572.0	lower Röt member	*V. heteromorphus*	100 (R)
14		572.5			50 (R)
15		574.5			50 (R)
16	W-VII/4W	297.0	?	?	70 (R)
17		333.5	upper Röt member	*M. fastidiosus*	2 (B)
18		360.5	lower Röt member	*V. heteromorphus*	50: 40 (R), 5 (B),1 (Z), 4 (P)
19	W-VII/6	444.0	upper Röt member	*M. fastidiosus*	70 (R)
20		448.0			70 (R)
21		525.0			20: 15 (R), 5 (B)
22	W-IX/6W	250.0	upper Röt member	*M. fastidiosus*	>1 (P)
23		296.0			>3: 2 (B), >1 (P?)
24		327.0			>0,5 (P)
25	W-XI/6W	61.5	Muschelkalk	*P. minor*?	15 (R + M)
26		91.5	?	?	100 (R)
27		153.0	upper Röt member	*M. fastidiosus*	1(B)
28		157.0	lower Röt member	*V. heteromorphus*	100: 97 (R), 1 (B), 1 (Z), 1 (P)
29	Raciborowice 1		upper Röt member	*M. fastidiosus*	0
30	Jerzmanice 1 top		Muschelkalk	*P. minor*?	40 (R + M)
31	Jerzmanice 1 base		?	?	80 (R)

Abbreviations: W-I/1 – borehole without core-sampling, W-I/3W – fully cored boreholes; 444.0 – sample from the cored section, B – miospores of the Lower Triassic *D. nejburgii* Zone, M – palynomorphs of the Middle Triassic *P. minor* Zone, P – Palaeozoic palynomorphs older than Permian, R – miospores of the Lower Triassic *V. heteromorphus* Zone, Z – miospores of the Lopingian *L. virkkiae* Zone.

The closely spaced borehole records, combined with seismic data, indicate that the Röt is limited to a relatively narrow (~3–5 km wide), NW–SE-elongated belt across the BS area (Fig. 2). This belt strikes obliquely in relation to the historically interpreted faults and fold-axes of the BS (e.g., Bałazińska and Bossowski, 1979; Berezowski and Berezowska, 1981). The Röt succession usually reaches 40 to 100 m in this area. It gradually thins to a few metres and pinches out toward the SW. In contrast, the NE to E limit of this area displays abrupt tectonic termination (Fig. 2).

Although the extent of the Röt succession is very limited within the study area (Fig. 2), its thickness varies considerably from 0 to about 180 m. Such striking thickness differences within a succession pose some questions concerning facies architecture, facies gradients, basin geometry, and incompleteness (stratigraphic gaps) of the succession and its potential tectonic deformation. Certainly, the gradual decrease in thickness toward the SW appears to be explained by a stratigraphic hiatus and erosional gap. This conclusion is supported by the incompleteness of the Röt succession, transected by some of the boreholes located in this area (Fig. 4). The most striking evidence of such a gap is provided by borehole W-V/6W, where its palynological documentation indicates that the entire Röt intersection is

represented exclusively by its lower member. An analogous conclusion came from analysing the corresponding wireline logs (Fig. 8). A similar incompleteness can be observed in some other boreholes (W-V/3, W-III/2 and W-I/3W), which are located in central parts of the Röt subcrop belt.

Strikingly, the lowermost part of the "standard" Röt succession (Fig. 7) also appears to be missing in some of the borehole sections, whereas its upper stratigraphic parts are present. Such a case was documented by the concurrent palynological and wireline log evidence in borehole W-III/2 (Figs 4, 8). Palynological data from two independent samples, collected in this borehole, indicate the upper Röt palynostratigraphy. The combined GR-RHOB wireline-log pattern from this borehole appears to indicate the absence of most of the lower to middle parts of the "standard" Röt wireline log profile. Similarly, only the palynological assemblages of the upper Röt have been documented in the lowermost parts of the Röt sections in boreholes W-III/4W and W-VII/6 (Fig. 4).

A few simplified composition maps have been compiled by application of the parameters derived from the wireline logs to illustrate the variability in composition of the Röt succession across the study area (Fig. 10). Relatively high concentrations of clay and quartz (standard wireline "minerals") are observed in the western part of the study area, while the amounts of them decrease gradually toward the E and NE (Fig. 10A, B). The concentrations of these two components correspond to the proportions of siliciclastic material within the Röt succession and reflect relative proximity to the terrigenous source areas. It appears that the distribution of combined quartz and clay displays a similar but slightly more consistent trend (Fig. 10C). Carbonates, in turn, are more abundant in the NE part of the area, while their lowest concentrations are observed along the NW, SE and SW peripheries of the area (Fig. 10D). The W-XI-4 borehole displays strongly "anomalous" concentrations of all the previously mentioned components. This anomaly is interpreted as being induced by local karstic processes, which caused the (fracture-preferred?) dissolution of a carbonate substrate and introduction of younger siliciclastic material along the fractures and into cavities.

Palynology

Three palynological assemblages were identified in the material examined, including both drill profiles and exposures (locations of the core palynological samples are indicated and labelled on Figs 3, 4). They are characterized by the varied content of damaged forms, belonging to the same palynological zone as the entire assemblage (marked with the letter R in Table 2), and redeposited from older deposits, namely the lower Buntsandstein (B), Zechstein (Z) and Palaeozoic, older Permian (P).

The oldest assemblage was found in five boreholes (Figs 3, 4; Tab. 2): W-I/3W (62.5 m), W-V/3 (65.0 m, 97.5 m), W-V/6W (572.0-574.5 m), W-VII/4W (360.5 m) and W- XI/6W (157.0 m). It is strongly dominated by pollen grains (over 80% of the total miospore count, on average), among which *Triadispora* specimens predominate, represented mainly by the species *T. crassa*. Specimens of *Illinites, Protohaploxypinus, Klasipollenites, Brachysaccus, Lunatisporites* (Fig. 11J) are less numerous, while specimens of *Angustisulcites, Striatoabietites, Stellapollenites, Platysaccus* and the species *Voltziaceaesporites heteromorpha* (Fig. 11I) as well as spores from the genera *Punctatisporites* (Fig. 11M), *Cyclotriletes, Lapposisporites, Kraeuseliposites* (Fig. 11S), *Aratrisporites* (Fig. 11T), *Verrucosisporites* with the species *V. thuryngiacus* (Appendix) occur singly. The W-V/3 (65.0 m) sample is distinguished by a relatively high proportion of spores, reaching 20%, while in the remaining samples it is several to 10%. The content of damaged miospores is high and amounts to 50%, while in the case of two samples: W-V/6W (572.0 m) and W-XI/6W (157.0 m), it reaches even 100% (Tab. 2). In three samples: W-I/3W (62.5 m), W-VII/4W (360.5 m) and W-XI/6W (157.0 m), miospores of *Densoisporites nejburgii* were found redeposited from the middle Buntsandstein deposits, in two samples: W-VII/ 4W (360.5 m) and W-XI/6W (157.0 m) specimens of *Lueckisporites virkkiae* (Fig. 12I) and in sample W-I/3W (62.5 m) also *Nuskoisporites dulhuntyi* and *N. klausii* (Appendix), redeposited from Zechstein sediments, and older undetermined miospores (Fig. 12J). In the W-V/3 sample (65.0 m), probably redeposited acritarchs of the genus *Veryhachium* (Appendix) occur sporadically.

The younger assemblage was recognized in most of the boreholes studied: W-I/1 (207.0 m), W-I/3W (33.0 m), W-III/2 (110.0 m), W-III/4W (382.0 m, 411.0 m, 418.0 m), W-VII/4W (333.5 m) W-VII/6 (444.0 m, 448.0 m, 525.0 m), W-IX/6W (250.0 m, 296.0 m, 327.0 m), W-XI/6W (153.0 m) and in the outcrop at Raciborowice 1 (Fig. 3; Tab. 2). It differs from the syndrome described above in displaying a better state of preservation of miospores. In most samples, the proportion of damaged forms is 1–2%, whereas in two samples from the Raciborowice Górne 1 exposure and from the W-I/3W well (33.0 m), they were not found at all. Only in three samples from the W-VII/6 borehole the proportion of them is high and amounts to 20% and 70%. Among the identifiable forms, representatives of the *Triadispora* genus (Fig. 11A) clearly predominate, the proportion of which is on average 40%. Pollen grains of *Microcahryidites* (*Protodiploxypinus*) are less numerous (on average 15%) and belong mainly to the species *M. fastidiosus* (Fig. 11B), less frequently *M. doubingeri* (Fig. 11C) and *M. sittleri*. They are accompanied by specimens of *Angustisulcites gorpii* (Fig. 11D), *A. klausi* (Fig. 11E) and *A. grandis* (Fig. 11F), *Klausipollenites* sp., *Brachysaccus ovalis* (Fig. 11H), *Illinites chitonoides* and *Alisporites* sp. Striatite pollen grains from the *Lunatisporites*, *Striatoabietites* and *Protohaploxypinus* genera (Fig. 11K) as well as the index species *Voltziaceaesporites heteromorpha* and the monosaccate pollen grain *Stellapollenites thiergartii* (Fig. 11L) are rarely encountered. Single spores belong to the species *Psilatriletes triassicus* (Fig. 11N) and the genera *Cyclotriletes* (Fig. 11O), *Guttatisporites* (Fig. 11P, Q), *Verrucosisporites* (Fig. 11R) and *Lapposisporites* (Fig. 11U; Appendix). Several specimens of green algae from the genera *Reduviasporonites* (Fig. 11X) and *Schizosporis* also were identified. Among the damaged forms, there are both miospores, which may belong to the same palynological zone. For example, there are specimens of *Cyclotriletes* (Fig. 12A), *Kraeuselisporites* (Fig. 12D) or *Protohaploxypinus* (Fig. 12F)

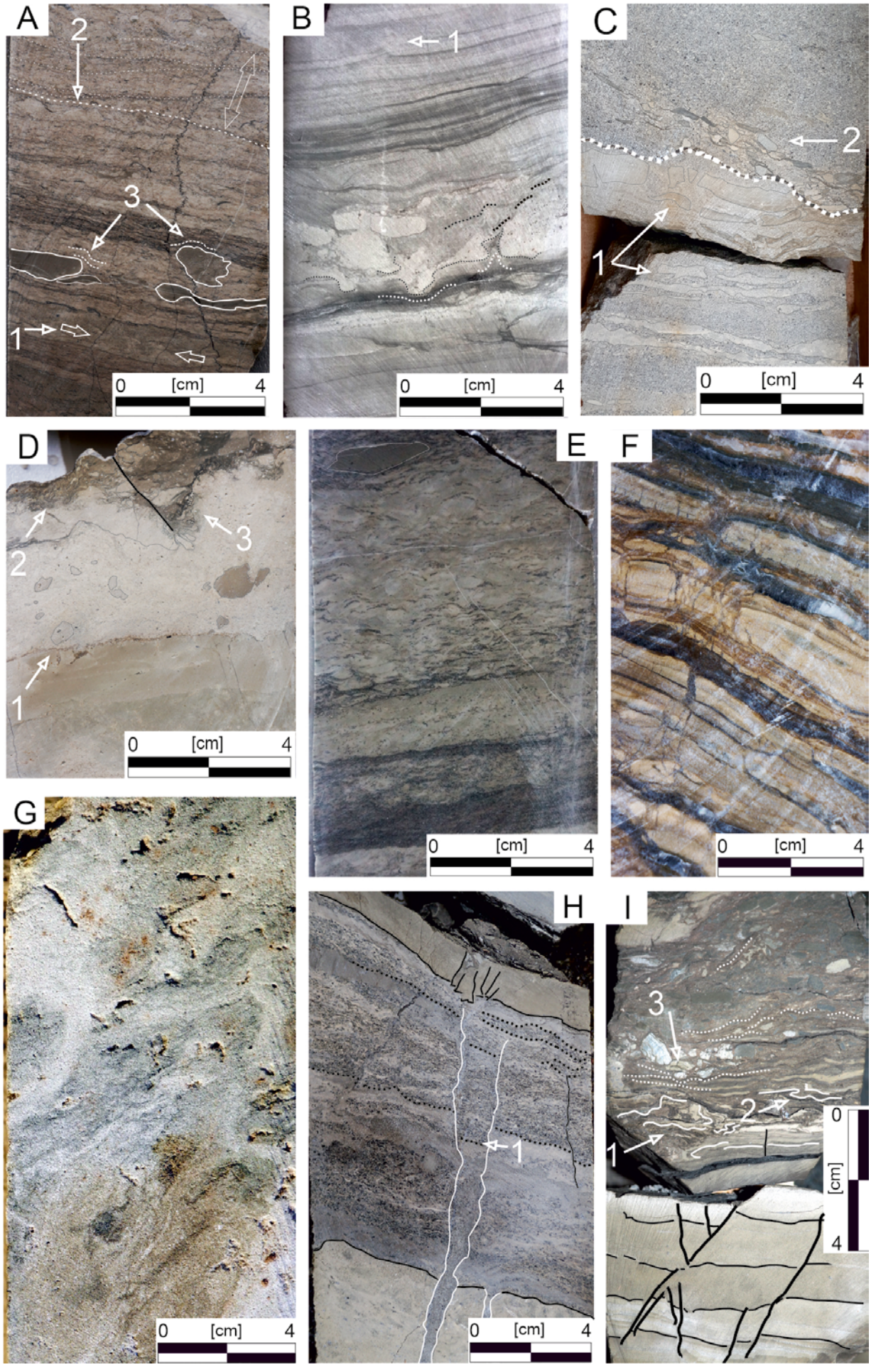
A
2
3
1
0 [cm] 4
B
1
0 [cm] 4
C
2
1
0 [cm] 4
D
2
3
1
0 [cm] 4
E
0 [cm] 4
F
0 [cm] 4
G
0 [cm] 4
H
1
0 [cm] 4
I
3
2
1
0
[cm]
4

Fig. 9.

and forms redeposited from older sediments. The latter include spores of *Densoisporites nejburgii* (Fig. 12G, H) and *D. playfordii*, pollen grains of *Lueckisporites virkkiae* (Appendix) and miospores, older than Permian (Tab. 2). In two samples, W-I/3W (33.0 m) and W-VII/6 (444.0 m), redeposited(?) acritarchs of the genera *Verychachium*, *Baltisphaeridium* and *Michrystridium* (Appendix) occur sporadically.

The youngest assemblage was found in two boreholes, W-I/1 (127.5 m, 200.0 m) and W-XI/6W (61.5 m), and in the top Jerzmanice 1 exposure. The content of damaged forms, which include only Triassic specimens (Fig. 12B, C, E), is 15–50% (Tab. 2). Among the well-preserved miospores, pollen grains of the genera *Triadispora* and *Microcahryidites* predominate, represented mainly by the species *M. doubingeri*. Less numerous are *Angustisulcites* specimens, dominated by *A. grandis, Stellapollenites thiergatii* and *Illinites chitonoides* (Fig. 11G). The remaining pollen grains (see Appendix) are found as single specimens. Among the spores, which make up from a few to 10% of spectra, representatives of the genera *Cyclotriletes, Puntatisporites* and *Verrucosisporites* predominate. Specimens of *Aratrisporites, Guttatisporites* and *Lapposisporites* are less common, and occasionally *Perotrilites mionor* occurs (Fig. 11V; Appendix). In the samples from the W-I/1 well, there is a microphytoplankton, making up 10% of the assemblage, which consists mainly of prasonophytes from the genera *Leiosphaeridia, Crassosphaera, Tasmanites* (Fig. 11W) and single acritarchs (Fig. 11Y; Appendix).

The analysed palynological samples generally are characterized by a low count of palynomorphs and poor preservation. These features are here provisionally attributed to sediment redeposition. The percentage of miospores that are damaged, although with no difference with respect to their colour intensity, varies between boreholes and appears to be related to the age of the assemblage. It is high in the oldest and youngest assemblage as well as in sample W-XI/6W (91.5 m), near the boundary of the Röt and Muschelkalk successions (Fig. 3; Tab. 2).

The processes of miospore deterioration have resulted in partial stripping of the exoexine layer, with an obvious impact on the elements of spore sculpture (Fig. 12A). Partial or even complete removal of the exoexine envelopes from some specimens of *Perotriletes minor* (Fig. 12B) and *Kraeuselisporites* sp. (Fig. 12C) significantly hindered their identification. Cracked (Fig. 12D) and torn specimens are also found. In the case of pollen grains, the results of partial destruction of exoexine are also observed. Very often, the air bags are damaged (Fig. 12E) or even detached from the central body of pollen. The central body also is often fractured (Fig. 12F).

Fig. 9. Selected depositional and deformational structures of the Röt of the Bolesławiec Syncline. **A.** Uneven planar parallel to wavy (?) lamination with sub-millimetre thick, dark-gray laminae and wisps (mud chips/fragments of algal mats?) of the organic-rich mudstone in a lime wackestone. Note the faint minute-scale load cast(?) deformations (arrow 1), thicker cross-stratified lamina with a tangential lower contact (arrow 2) and compaction-related bending of the lamination near intraclasts of the dark gray mudstone (arrows 3). The rock is cross-cut by irregular, almost perpendicular to stratification stylolites and probably affected by dissolution/recrystallization processes. Borehole W-IX/6W, depth 273.0 m. **B.** Planar parallel to wavy lamination in a mixed-composition marly limestone. Subangular to subrounded fragments of light grey lime grainstone, (due to localized breakage of a semi-consolidated sediment ?) float in a dark grey, poorly sorted matrix. Note a small-scale, faint fluidization plume (arrow 1) above the cuspate crack (syneresis?). Borehole W-VII/4W, depth 355.4 m. **C.** Intraformational breccias within diffusely stratified bioclastic limestone. The lower layer of breccia is monomictic (arrow 1) and encompasses large angular fragments of the light beige lime mudstone; fragments did not experience significant transportation; some of them appear to be "frozen" near their sites of origin. The upper layer of the breccia is polymictic (arrow 2) and includes smaller intraclasts of dark grey mudstone, marl and light beige limestone; this breccia layer overlies an erosional surface (dashed line). Borehole W-I/3W, depth 64.8 m. **D.** Irregular contacts between thin layers of compositionally/texturally different limestone. The lower contact (arrow 1), above the beige, parallel-laminated lime mudstone is partly lined-up with a veneer of a brownish wackestone and displays a few cross-sections of minute cracks and furrows. These features are typical for surfaces of lithification/hardground(?) and partial dissolution. The upper contact (arrow 2), above light beige layer of a mixed bio-to-intraclast lime encompasses slightly larger-scale irregular depressions filled-up with a brownish grey, poorly sorted marly matrix and angular fragments of light-beige substrate-derived limestone. This surface is interpreted as resulted from hardground development and/or incipient karst processes. It locally displays a thin zone of micritization (arrow 3). Borehole W-IX/6W, depth 285.0 m. **E.** Thinly bedded, marly limestone with diffuse parallel stratification (secondary?). The primary structural features are strongly obliterated by bioturbation burrows? and moderately advanced dolomitization. Note a large, flat subangular fragment of a dark grey lime mudstone in the uppermost part of the photo. Borehole W-III/4W, depth 412.0 m. **F.** Thinly interbedded to laminated limestone (light brownish to beige) and gypsum (dark grey to almost white). Interbedding of these two contrasting lithologies results in a distinct, banded character of the rock formation. The limestone layers/laminae display a very prominent, thin parallel (cryptalgal?) lamination. Note numerous micro-fractures, mostly perpendicular to lamination, which are filled-up with gypsum. Borehole W-IX/6W, depth 321.4 m. **G.** Strongly irregular internal structure due to advanced liquefaction and/or bioturbation (?) of a fine-to-medium grained sandstone. Borehole W-V/6W, depth 581.7 m. **H.** Small-scale neptunian dyke cutting across crudely laminated, bioclastic marl (dark grey) and the underlying marly limestone wacke (beige). Internal infill of the dyke displays well preserved graded bedding which locally appears to be displaced down into the dyke (arrow 1) with respect to its shoulders. Borehole W-XI/6W, depth 135.0 m. **I.** Complex zone of fold-like deformations (continuous and detached) and intraformational breccia above layer of a light beige lime mudstone, which displays fracture/microfault pattern typical of extensional-style deformations. Small-scale, microslump-like (arrow 1) and drag (arrow 2) folds affected the basal part of the deformational package, which consists of discontinuously laminated lime mudstone and marly wackestone (darker grey). Slight compactional bending of lamination around larger clasts is indicated by arrow 3. The upper part of the package is represented by a polymictic intraformational breccia with an abundant muddy matrix. Borehole W-V/6W, depth 581.0 m.

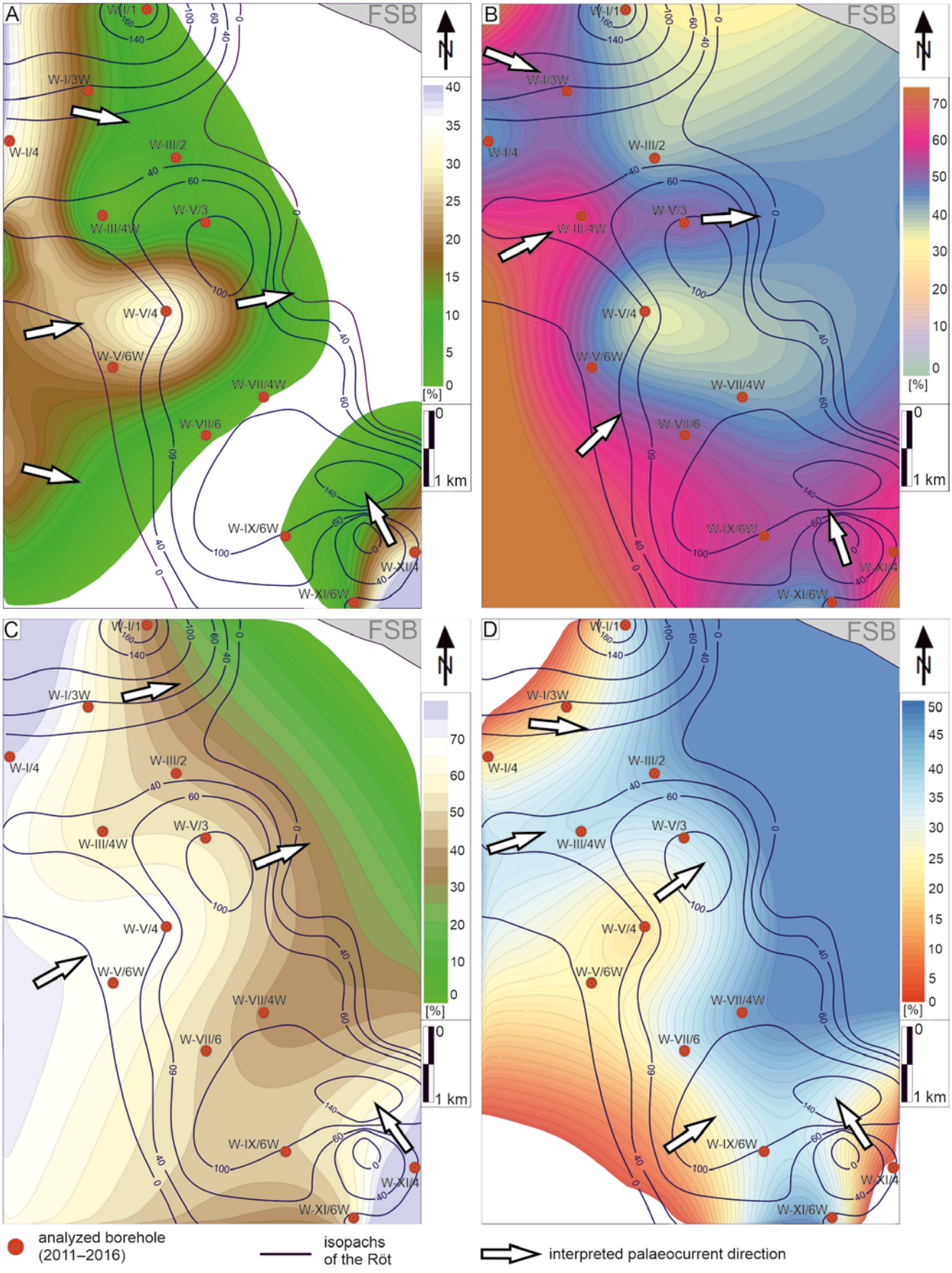

Fig. 10. Component percentage maps of the Röt succession of the study area: quartz (A); clay (B); quartz + clay (C); carbonate (D); all components are apparent wireline-log minerals. FSB - Fore-Sudetic Block.

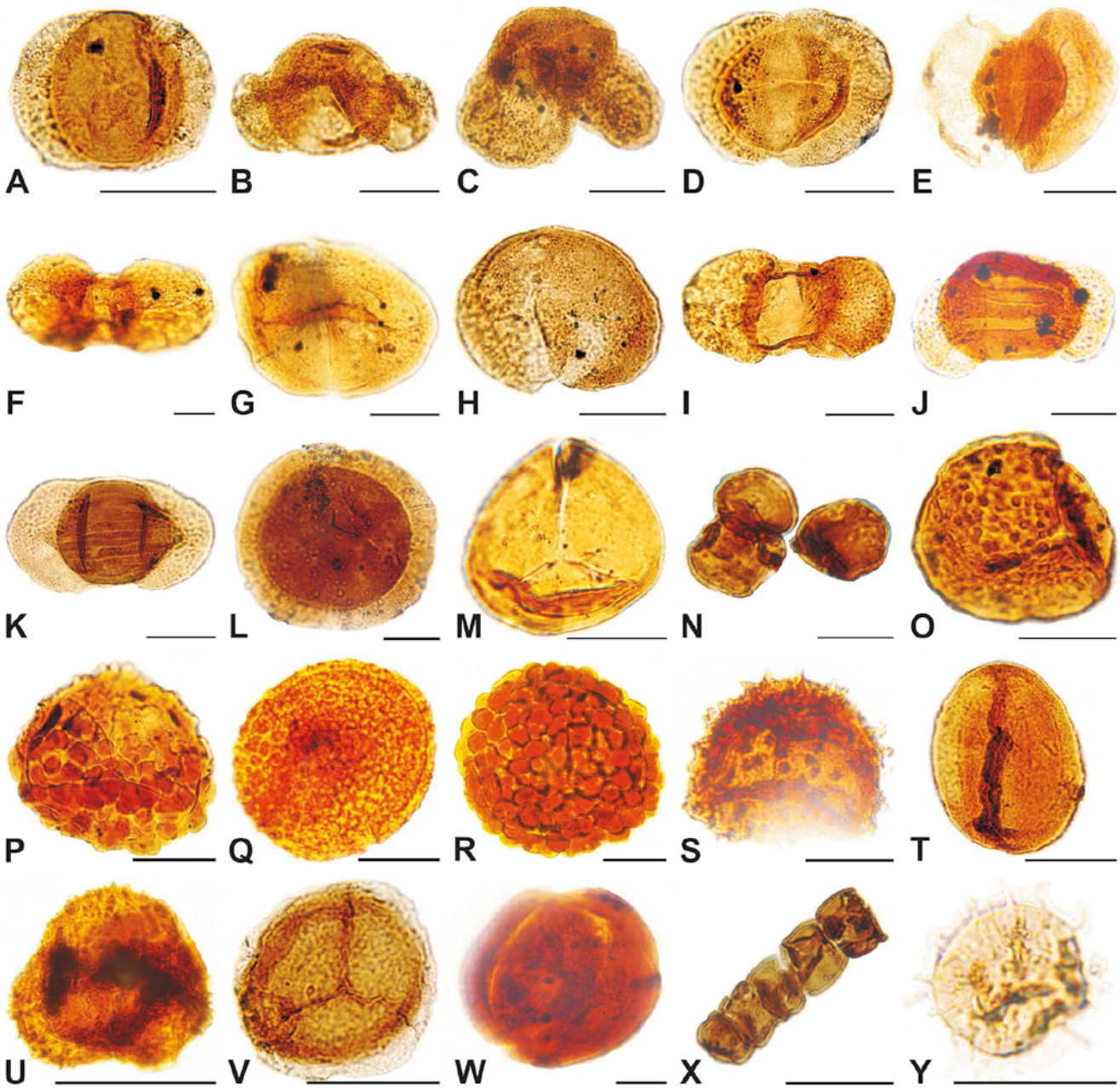

Fig. 11. Palynomorphs from the Röt and Muschelkalk deposits of the Bolesławiec Syncline. **A.** *Triadispora crassa* Klaus, W-IX/6W borehole, depth 250.0 m, upper Röt member, slide 1 (s1), Y66,4 (English finder coordinates). **B.** *Microcahryidites fastidiosus* (Jansonius) Klaus, W-VII/6, 444.0 m, upper Röt member, s1, Q43 **C.** *Microcahryidites doubingeri* Klaus, W-IX/6W, 327.0 m, upper Röt member, s1, C39,4. **D.** *Angustisulcites gorpii* Visscher, W-IX/6W, 296.0 m, upper Röt member, s1, S57,1. **E.** *Angustisulcites klausi* Freudenthal, W-I/3W, 33.0 m, upper Röt member, s1, Z36,1. **F.** *Angustisulcites grandis* (Freudenthal) Visscher, W-VII/4W, 333.5 m, upper Röt member, s2, Y44,3. **G.** *Illinites chitonoides* Klaus, W-I/1, 200.0 m, Muschelkalk, s1, G42,2. **H.** *Brachysaccus ovalis* Mädler, W-IX/6W, 296.0 m, upper Röt member, s2, V46,3. **I.** *Voltziaceaesporites heteromorpha* Klaus, W-IX/6W, 296.0 m, upper Röt member, s1, I50,3. **J.** *Lunatisporites gracilis* (Jansonius) Fijałkowska, W-V/6W, 572.0 m, lower Röt member, s2, E43. **K.** *Protohaploxypinus samoilovichii* (Jansonius) Hart, W-VII/6, 525.0 m, upper Röt member, s1, M54,3. **L.** *Stellapollenites thiergartii* (Mädler) Clement-Westernhof, W-IX/6W, 250.0 m, upper Röt member, s1, Z44, 1. **M.** *Punctatisporites triassicus* Schilz, W-V/3, 97.5 m, lower Röt member, s2, P59,4. **N.** *Psilatriletes triassicus* Visscher, W-VII/6, 525.0 m, upper Röt member, s1, M50. **O.** *Cyclotriletes triassicus* Mädler, W-VII/4W, 333.5 m, upper Röt member, s1, V58. **P.** *Guttatisporites elegans* Visscher, W-XI/6W, 153.0 m, upper Röt member, s1, Q39,2. **Q.** *Guttatisporites microechinatus* Visscher, W-VII/4W, 333.5 m, upper Röt member, s1, V52. **R.** *Verrucosisporites thuryngiacus* Mädler, W-VII/4W, 333.5 m, upper Röt member, s1, J54,4; **S** – *Kraeuselisporites* sp., W-V/6W, 572.5 m, lower Röt member, s2, G35. **T.** *Aratrisporites granulatus* Klaus, W-VII/4W, 360.5 m, lower Röt member, s1, V50. **U.** *Lapposisporites villosus* Visscher, W-VII/4W, 333.5 m, upper Röt member, s2, F50,1. **V.** *Perotrilites minor* (Mädler) Antonescu et Taugordeau-Lanz, W-I/1, 127.5 m, Muschelkalk, s1, Y59. **W.** *Tasmanites* sp., W-I/1, 200.0 m, Muschelkalk, s2, P25. **X.** *Reduviasporonites catelunatus* Wilson, W-IX/6W, 327.0 m, upper Röt member, s1, Q42,3. **Y.** *Michrystridium* sp., W-XI/6W, 61.5 m, Muschelkalk, s1, C53.

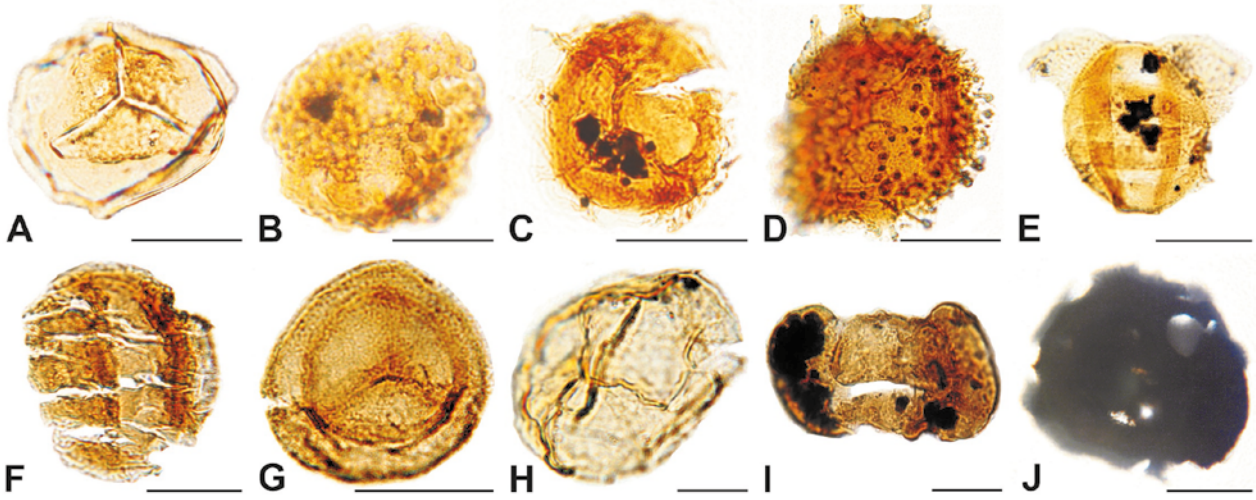

Fig. 12. Damaged, redeposited and reworked miospores from the Röt and Muschelkalk deposits of the Bolesławiec Syncline. **A**. *Cyclotriletes* sp., W-IX/6W, 327.0 m, upper Röt member, sl, X29,2. **B.** *Verrucosisporites* sp., W-I/1, 127.5 m, upper Röt member, sl, W51,1. **C.** aff. *Perotrilites* sp., W-XI/6W, 61.5 m, Muschelkalk, s2, V57. **D.** *Kraeuselisporites* sp., W-VII/4W, 333.5 m, upper Röt member, sl, S49,4. **E.** *Lunatisporites puntii* Visscher, W-I/1, 200.0 m, Muschelkalk, sl, M38,4. **F.** *Triadispora* sp., W-VII/6, 525.0 m, upper Röt member, s2, T60,4. **G, H.** *Densoisporites nejburgii* (Schulz) Balme, W-VII/4W, 333.5 m, upper Röt member, sl, G – V41,3, H – K45. **I.** *Lueckisporites virkkiae* Potonié et Klaus, W-VII/4W, 360.5 m, lower Röt member, sl, V57. **J.** undetermined spore, W-XI/6W, 157.0 m, lower Röt member, s2, P59.

In addition to the damaged miospores, there also occur a few reworked palynomorphs, which are older than the age of the main sample spectrum and usually display a darker colour. This includes spores of the genus *Densoisporites* with the species *D. nejburgii* (Fig. 12G), indicative of the zone distinguished in the middle Buntsandstein deposits of Poland (Orłowska-Zwolińska, 1984, 1985). The reworked pollen of the species *Lueckisporites virkkiae* (Fig. 12H) are indicative of the zone, distinguished in the Zechstein deposits in Europe (Visscher, 1974, 1980), as is the case for the late Permian monosaccate pollen *Nuskoisporites dulhuntyi* (Fig. 12I) or the bisaccate pollen of the genus *Jugasporites* (Appendix). The analysed samples also contained a number of highly carbonized spores (Fig. 12J), the taxonomy of which cannot be determined.

The miospore assemblages, described above, represent two palynostratigraphic zones: *Voltziaceaesporites heteromorpha* and most probably *Perotriletes minor* (Tab. 2), established by Orłowska-Zwolińska, (1984, 1985) in the upper Olenekian – lower Anisian deposits of Poland. The *V. heteromorpha* and *P. minor* zones are correlated with the *T. crassa – Verrucosisporites* Zone and the lower part of the *Stellapollenites thiergartii* Zone of Kürschner and Herngreen (2010) respectively, with the sixth and seventh and lower part of the eight zone of Heunisch (1999), recognized in the Röt and Muschelkalk deposits of the Germanic Basin. Additionally, in the upper part of the *V. heteromorpha* Zone, there is the *Microcahryidites fastidiosus* Subzone, which can be correlated with the *P. leschiki* Subzone of Kürschner and Herngreen, (2010; Fig. 3). It is worth emphasizing that the taxonomic composition of the youngest assemblage is more similar to the *Protodiploxypinus doubingeri* Zone of Kürschner and Herngreen (2010) and eight zone of Heunisch (1999) than to the Polish *Perotrilites minor* Zone of Orłowska-Zwolińska (1985).

Elements of subsurface topography and tectonic deformation

The upper surface of the siliciclastic Buntsandstein facies (tTb), which underlies the Röt succession in the study area, displays a strongly diversified topography (Fig. 13). This surface dips uniformly toward the SW and W across the SW part of the study area. Toward the ENE, beyond the Röt subcrop area, it flattens and forms a narrow elevation/ridge (Fig. 13), where the Buntsandstein is partly eroded and overlain by younger Tertiary to Quaternary sediments (Fig. 14B, C). However, the subsurface topography of the tTb boundary is locally much more diversified and displays a few prominent depressions and elevations with absolute differences in elevation reaching up to about 200–400 m (Fig. 13). The most prominent of these subsurface forms occurs in the NW part of the study area, where the tTb surface drops substantially in level. This NW–SE-elongated tTb subsurface depression is separated by a narrow ridge from the main, uniformly SW-dipping area (Fig. 13). The crest of this ridge is slightly undulating, but it generally dips at a very shallow angle toward the NW. Noticeably, the underlying siliciclastic Buntsandstein succession thickens significantly and reaches up to 700–850 m beneath this ridge (Fig. 13), while its thickness varies between 450 and 550 m across most of the study area (Fig. 14). Several of the most nearly complete and thickest borehole intersections of the Röt succession occur within the local, small-scale depressions of the tTb subsurface (Fig. 13). All the known occurrences of the Muschelkalk carbonate rocks in the area also coincide with these subsurface depressions (Fig. 13).

The subsurface topography of the tTb boundary is very well illustrated by 2D reflection seismic data (Fig. 14A–C). The cross-section I–I' (Fig. 14A) depicts the main features of the local geological structure along a SW–NE line in the

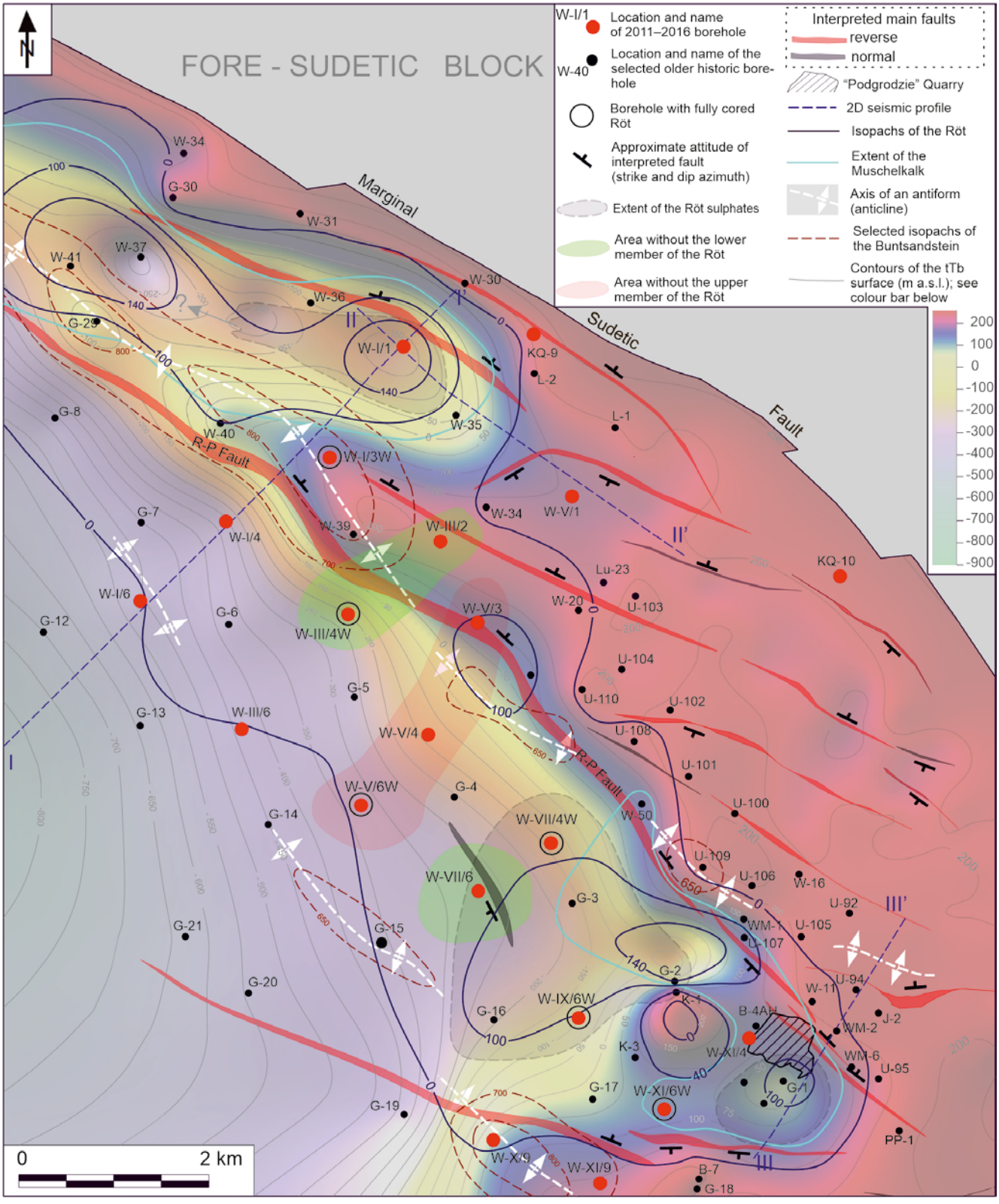

Fig. 13. Complex structural-facies map of the Röt and Buntsandstein in the Bolesławiec Syncline.
Abbreviations: R-P Fault – Raciborowice-Parowa Fault; tTb – top of the Buntsandstein surface.

NW part of the study area (see Figure 13 for location). The prominent tTb subsurface depression with a complex, synclinorial character is clearly visible in the NE part of this cross-section. Also, a corresponding elevation, which displays a complex thrust-fault-like internal structure, appears in the central-to-NE part of the same section (Fig. 14A). It seems quite obvious that the significant thickness increase of the Buntsandstein succession, associated with this elevation, is related to thrust-fault tectonics (Fig. 14A; see also Fig. 13). It is noteworthy that a minor elevation of the

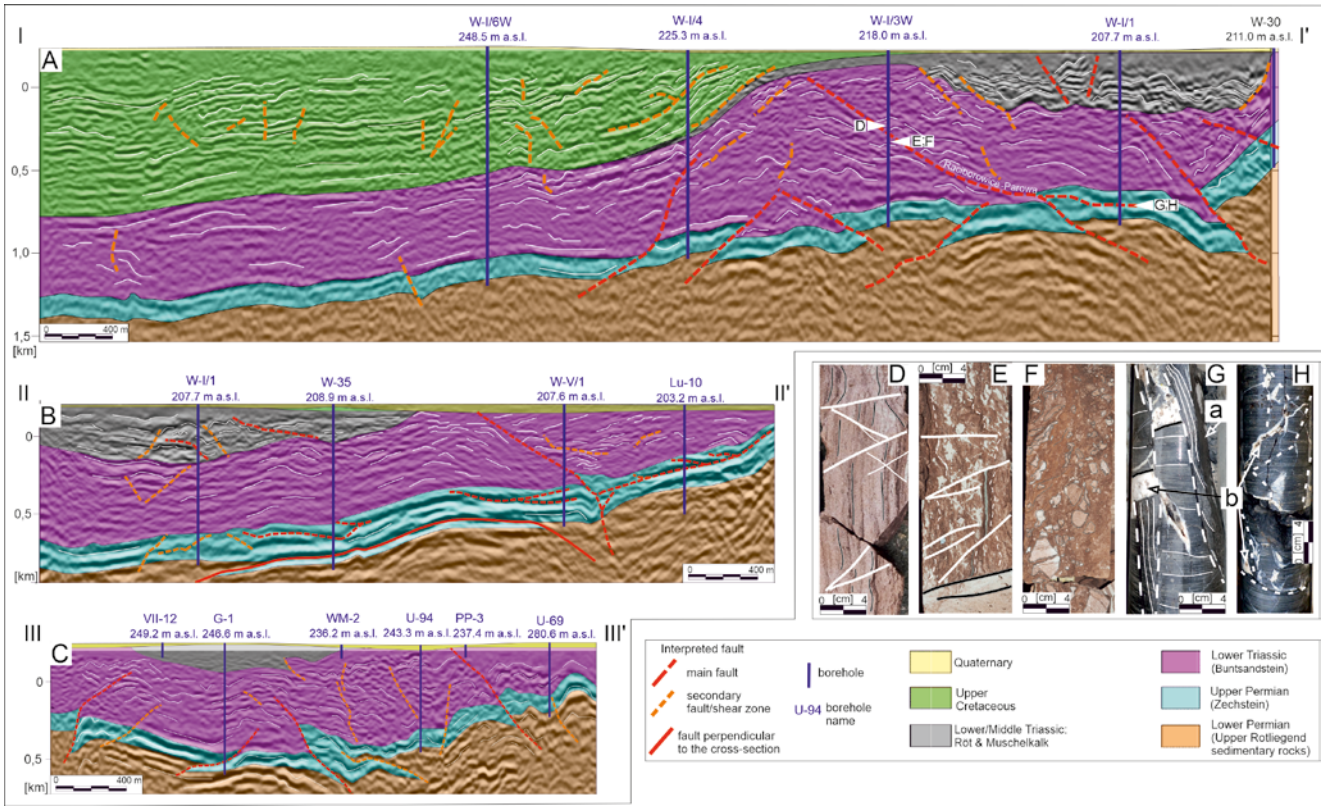

Fig. 14. Selected seismic cross-sections (A, B and C) of the Bolesławiec Syncline (for location see Figure 12*;* cross-section A modified after Durkowski, 2022). Inserted core photographs (D through H) depict selected examples of tectonic deformations, encountered within the Buntsandstein and Zechstein successions (for location, see Figure 12).

same stratigraphic surface appears about 1.5–2 km further south-westwards, near the projection of borehole W-I/6W (Fig. 14A, see also Fig. 13). This lesser elevation does not correspond to any swelling of the Buntsandstein strata but appears to be related to local tectonic faulting and folding (Fig. 14A). Independently, this minor elevation occurs along the NW extension of a less distinct belt of increased thickness of the clastic Buntsandstein succession, which appears to run roughly parallel to the first one (Fig. 13).

It is worth noting that most of the borehole sections of the Buntsandstein succession usually are without any deformational structures of a tectonic nature. However, numerous deformations of such a nature (normal and inverse faulting, steep structural dips) and a common brecciation have been observed in some of the modern boreholes (W-X/9, W-I/3W, W-XI/9, W-III/2; Fig. 14D–H) and appear to be related to younger, post-Triassic tectonic deformation. The descriptions from some of the older, historic boreholes (G-15, W-39, W-40, W-50) also refer to numerous deformational structures of apparent tectonic nature within the siliciclastic Buntsandstein succession. All the above-mentioned boreholes were completed in areas of significantly increased thickness of the Buntsandstein facies (Fig. 13).

DISCUSSION

The contact of the Buntsandstein and Röt successions locally appears to have almost a transitional nature and was placed above a thick fining-upwards sequence of the uppermost Buntsandstein facies (Figs 3, 8). However, in many boreholes, the contact of these two successions is abrupt and the carbonate Röt sediments overlie a contrasting sandy substrate of the Buntsandstein facies (e.g., W-III/2; see Figs 4, 8). Thus, the basal Röt sediments overlie distinctly different facies of the Buntsandstein in the study area. Additionally, the basal parts of the Röt succession display the younger Röt palynostratigraphic assemblage in some boreholes (Figs 3, 4, 8; see also Tab. 2). Thus, the Triassic succession of the BS appears to encompass locally a stratigraphic gap, approximately at the boundary between the Röt and Buntsandstein successions.

Similar gaps between the Buntsandstein and Röt have been recognized in other parts of the Germanic Basin. Geluk (2005) and others (Bachmann *et al.*, 2005; Geluk and Rohling, 1997) have demonstrated that the Lower Triassic succession also includes a few significant stratigraphic unconformities and gaps in the Thüringen and Lower Saxony areas. The presence of a significant discontinuity near the Buntsandstein-Röt boundary must be interpreted as occurring along the margins of the Polish-Danish Trough, central to NE Poland (cf. Senkowiczowa, 1965; Szyperko-Śliwczyńska, 1980; Szyperko-Teller, 1997). That area experienced significantly increased subsidence during the Early Triassic, which resulted in the greater thickness of the Buntsandstein facies (Dadlez *et al.*, 1998; see also Geluk, 2005). The younger Röt rocks overlie the Buntsandstein substrate discordantly along the surface, which may be

interpreted as resulting from onlap. It closely resembles a transgressive overlap *sensu* Krumbein and Sloss (1963, figs 9–5; cf. Szyperko-Śliwczyńska, 1980, fig. 2; Szyperko-Teller, 1997, fig. 34).

A few boreholes, located in the north-western area of the NSS, appear to provide clear documentation of a gradual transition (concordant contact?) from the Buntsandstein to the Röt facies (Sokołowski, 1967; Durkowski *et al.*, 2017). The topmost part of the Buntsandstein facies, which consists of predominant light-grey sandstone, usually includes lenses and interbedded layers of carbonate rocks with admixed glauconite (e.g., boreholes Bolesławiec N-24, Osieczów N-25, Wykroty N-14; Fig. 1A). The corresponding top-Buntsandstein facies are without such components in the eastern BS area. In turn, this light-grey sandstone is commonly overlain by a rusty, clay-rich, regolith-like/transgressive layer (Fig. 6A) or deformational packages (Durkowski, 2022). Such contact relationships indicate that the depositional surface of the NSS area was considerably diversified before the onset of sedimentation of the Röt facies; specifically, higher elevations predominated in the ESE part of the NSS area, as compared to its north-western areas. This indicates that the Röt transgression within the NSS sub-basin progressed gradually from the NW toward the SE. Consequently, the base-of-Röt surface does not have a time-stratigraphic character. Such a relationship may be applicable to almost the entire Germanic Basin, where some of its central parts apparently had been dominated earlier by calcareous Röt sediments and experienced some invasions of siliciclastic material from marginal regions (cf. Szulc, 2000).

The 2D seismic data demonstrate that the Triassic deposits exhibit zones of strong tectonic deformation and relative uplift (Fig. 14). Some folds display complex internal structures, obviously related to thrust-style displacements and strong fracturing along their axial planes (Fig. 14A, C). The WNW–ESE to NW–SE orientation of the interpreted fold axes and the inverse steep faults parallel/sub-parallel to them (Figs 5, 12) are interpreted as being roughly perpendicular to the principal compressional stress, related to these deformations. One cannot exclude the possibility that the late compressional-style tectonic fabric locally overprints earlier tectonic features, such as late/post Variscan and/or Early Triassic normal faults and grabens, related to extensional tectonic settings (Sokołowski, 1967; Krzywiec, 2004; Patruno *et al.*, 2020). Some relics of these early features can be observed at lower stratigraphic levels (Permian) of the seismic cross-sections of the BS (Fig. 14). However, the final suite of folding, steep reverse faulting and incipient thrusting the authors interpret as being related to much younger, most likely Late Cretaceous inversion in conditions of a compressional (or transpressional) regime, as postulated for Central Europe (e.g., Mazur *et al.*, 2005; Kley and Voigt, 2008). The compressional-style deformations of the BS area clearly embrace the entire Permo-Mesozoic succession, including its Permian, Triassic and Upper Cretaceous segments (Fig. 14A). However, a significant imprint of strike- to oblique-slip (sinistral?) displacements (Fig. 13) cannot be excluded at this stage of the study.

The character of the North-Sudetic Triassic succession and its sequence organisation seems to confirm a general basin-wide (Germanic Basin) tendency in the development of its sedimentary succession. A change from the continental conditions of the Buntsandstein facies to marine ones of the Röt-Muschelkalk facies appears to be related to the pre-existing topography and was preceded by significant tectonic movements. However, these tectonic events did not occur simultaneously within the various compartments of the complex Germanic Basin. The late to end Buntsandstein phases witnessed strong extensional tectonics, differential subsidence and local rifting of several parts of this basin (e.g., Patruno *et al.*, 2020). Some corresponding events took place, most likely, more-or-less simultaneously within the adjoining northern parts of the coexisting Tethys Ocean. Recently, Jaglarz and Rychliński (2018) documented a set of distinct surfaces of emergence and/or non-deposition, as well as evidence of the development of karstic processes and solution breccias within the late Olenekian and Anisian Tethys carbonate succession of the Tatra Mts., southern Poland. The Triassic succession of the BS displays numerous features, similar to and apparently coincidental with some other areas of the Germanic Basin. However, the timing of particular events on local scales was, most likely, slightly different.

Some features of the Röt depositional system of the BS certainly were inherited from the predecessor phase of continental sedimentation of the Buntsandstein facies. Mroczkowski (1969, 1972) provided quite convincing evidence, concerning the palaeocurrents during sedimentation of the Buntsandstein siliciclastics in the broader area of the NSS. The corresponding palaeotransport indicators point consistently to a NNE-ward inclination of the palaeoslope across the entire area.

Some indicators presented in this article suggest that the general NNE trend of the depositional palaeoslope persisted also during sedimentation of the Röt facies across the study area. The most important indicator is related to the thickness distribution of the Röt succession, which systematically increases from the SW toward the NE across a significant part of the area (Figs 2, 13). It is worth noting that the NE termination of the Röt belt and its abrupt thickness reduction are due to a significant tectonic uplifting and subsequent erosion. In turn, the gradual SW termination of the Röt sub-crop area was accompanied by limited tectonic deformation and appears to never have been significantly elevated, although it is obviously partly eroded (Fig. 14A). The Triassic deposits in that area are buried under the thick and uniform succession of the Upper Cretaceous, thus, potential uplift and related erosion of the younger deposits (Upper Triassic and younger?) may be dated as pre-Cenomanian (cf. Leszczyński, 2018). A set of provisional composition maps of the Röt (Fig. 10) appears to corroborate the above-mentioned tendency of thickness distribution.

Several independent indicators strongly suggest that the physiography of the Röt basin in the study area was diversified on a small scale. The absence of the lower part of the Röt succession in particular boreholes can be interpreted in terms of either pre-upper Röt erosion or non-deposition. Accordingly, the absence of its upper part resulted from either non-deposition or later erosion. Simultaneously, the subsurface extent of the Muschelkalk rocks in the study

area is even much more limited than that of the Röt succession (Fig. 13). However, it is not clear to what degree such a limited extent of the Muschelkalk succession is related to non-deposition or the post-Muschelkalk (pre-Late Cretaceous) erosion.

It is noteworthy that the Röt succession in borehole W-I/1 is approximately twice as thick as in any other of the newly completed boreholes (Figs 2, 4, 7). One might suspect that this anomaly might have resulted from the younger tectonic deformations (over-thrusting and sequence repetition). However, the close similarity of the GR/RHOB sequence patterns, recorded in boreholes W-I/1 and W-XI/6W, indicate that contrasting differential subsidence has been at least partly responsible for such differences. It could be suggested that a precursor of the prominent, NW-SE-striking Raciborowice-Parowa fault (Fig. 13) might have played an important role in tectonic compartmentalization and subsidence differentiation during sedimentation of the Buntsandstein and Röt deposits. The present-day geometry and character of this fault (Fig. 14A) is related, most likely, to the later stages of basin inversion. Independent borehole documentation indicates that the Raciborowice-Parowa fault continues significantly further toward the NW over the area of the western NSS (boreholes Bolesławiec N-24, Osieczów N-25 and Parowa N-27; Fig. 1A).

Numerous small-scale deformational structures were encountered within the lower parts of the Röt borehole sections ("main deformed interval" of Durkowski, 2022). They are accompanied commonly by small-scale gravity/mass re-deposition packages. Both the frequency and intensity of deformations decrease up the Röt succession until their complete absence in the Muschelkalk carbonate deposits (Figs 3, 4). Such an evident dependence on stratigraphy of the deformational structures within the entire Triassic succession and their strong tendency to be hosted by the lower part of the Röt succession indicate their potential association with the synsedimentary tectonic activity.

The high-frequency lithological variability of the Röt succession is accompanied by the occurrence of very common intraclasts and numerous soft-sediment deformational structures. These features indicate that the depositional conditions varied frequently within the basin and a background slow accumulation of clay- and/or carbonate-rich sediments was frequently interrupted and punctuated by episodes of significantly faster deposition. These episodes were either related to significantly increased input of clastic material from the basin margins (and their limited cannibalisation) or remobilization and local mass re-deposition of fresh, unconsolidated sediment.

The common occurrence of intraclasts within the lower Röt rocks points to frequent episodes of erosion, which were followed by their short-distance transportation and re-deposition. Interestingly, even deeper erosion of the pre-existing Lower Triassic deposits (Buntsandstein facies) within the limits of the nearby (?) source areas/basin shoulders, appears to be demonstrated by discoveries of miospore taxa of Early Triassic age, i.e., originating from the older Buntsandstein facies (see "Palynology"; Appendix 1). Local deeper erosion of the source areas also is evidenced by the occurrence of damaged and re-deposited (?) pollen and spores (Fig. 12).

It is worth mentioning that the impact of synsedimentary seismic activity on the carbonate Muschelkalk deposits of the Silesian-Małopolska and Holy Cross regions already has been demonstrated and discussed by Szulc *at al.* (2015) and Matysik and Szulc (2019). Despite the slightly younger age of those deposits, some broad regional relationships, and similarities with the calcareous Röt succession of the BS area appear to exist. Both areas demonstrate similar sedimentary end-products of a long-lasting, probably multi-phase process of their tectonic disassembling. The timing and intensity of those tectonic movements varied considerably across the affected area.

CONCLUSIONS

New, comprehensive description and analysis of the Röt sedimentary succession of the BS, NSS, allowed some significant updates on local geology and modifications of the corresponding geological record by younger tectonic deformation. The most important concluding remarks are as follows:

1. Sedimentary features of the Röt succession point to a predominant, slow-rate sedimentation from suspension and weak traction currents/wave action, which were punctuated by events of faster-rate sediment accumulation and redeposition of fresh, unconsolidated sediments.
2. Spatial trends in rock composition point to an overall NE inclination of the palaeodepositional slope within the BS basin area during the Röt sedimentation, which appears to closely mimic the inclination of depositional slope from the preceding period of its continental (Buntsandstein) stage. The physiography of the Röt sedimentary basin was diversified and reflected local tectonic influences, which led to its small-scale compartmentalization. It appears that the Röt marine transgression invaded the deeper, NW part of the NSS basin earlier and then, proceeded gradually toward the SE (BS area).
3. The onset of marine Röt sedimentation in the BS area was accompanied by the preferred development of diversified, small-scale deformational structures and mass re-deposition packages, common intraclasts and redeposited, older pollen/miospores.
4. It is postulated that synsedimentary tectonics/seismic activity, which resulted in significant faulting of the area, was a principal factor responsible for the local strong differential subsidence and the resultant differences in sediment accumulation rates.
5. The collected palynological material provided an indication of the latest Olenekian-early Anisian timing of the local Röt facies sedimentation.
6. Palynological data and correlation of wireline logs/sequence organisation have demonstrated that several borehole records of the Röt succession are stratigraphically incomplete. The authors interpret such local, lithostratigraphic "gaps" as resulting not solely from erosion and/or local non-deposition episodes, but some of them are probably related to late tectonic deformation.
7. The consistent thinning of the Röt succession along the southernmost edge of the present-day Röt subcrop belt

appears to approximate the original southwestern extent of the sedimentary basin compartment of the BS.

8. The basal surface of the Röt succession is regarded as a surface of transgression, which locally has an erosional character. This local unconformity appears to correspond stratigraphically to the basal Solling unconformity, as defined in other parts of the Germanic Basin (Bachmann and Kozur, 2004), although verification of this will require more precise bio- or magnetostratigraphic dating.
9. Both the Röt and underlying Buntsandstein successions were locally uplifted and display clear evidence of tectonic folding. This compressional-style deformation stage is tentatively interpreted as related to a stage of significant tectonic inversion, which post-dates the youngest Cretaceous rocks of the area.
10. The documentation and analysis presented constitute a framework for a more advanced and complete geological analysis of the Röt succession of the BS area, which will require careful sedimentological facies analysis and stratigraphic dating. Only then would an understanding of the Röt basin character, conditions, and development be satisfactory.

Acknowledgements

The authors would like to thank the ASGP reviewers for their critical reading and valuable comments. They provided us with a great deal of help in the substantial improvement of our manuscript and clarification of many of the ideas included. The authors would like to thank KGHM Polska Miedź S.A. for providing the material for the research.

REFERENCES

Anketell, J. M., Cegła, J. & Dżułyński, S., 1970. On the deformational structures in systems with reversed density gradients. *Rocznik Polskiego Towarzystwa Geologicznego,* 40: 3–30.

Asquith, G. & Gibson, C., 1982. Basic well log analysis for geologists. *American Association of Petroleum Geologists – Methods in Exploration Series.* Tulsa, 216 pp.

Assmann, P., 1944. Die Stratigraphie der oberschlesischen Trias. Teil II – der Muschelkalk. *Abhandlungen des Reichsamts für Bodenforschung*, 208: 1–124.

Bachmann, G. H. & Kozur, H. W., 2004. The Germanic Triassic: correlations with the international chronostratigraphic scale, numerical ages and Milankovitch cyclicity. *Hallesches Jahrbuch für Geowissenschaften*, 26: 17–62.

Bachmann, G. H., Beutler, G., Szurlies, M., Barnasch, J. & Franz, M., 2005. *International Workshop on the Triassic of Germany and Surrounding Countries*. M. Luther Universität Halle-Wittemberg, 76 pp.

Bachmann, G. H., Geluk M. C., Warrington, G., Becker-Roman, A., Beutler, G., Hagdorn, H., Hounslow, M. W., Nitsch, E., Röhling, H.-G., Simon, T. & Szulc, A., 2010. *Triassic.* In: Doornenbal, J. C. & Stevenson, A. G. (eds), *Petroleum Geological Atlas of the Southern Permian Basin Area.* EAGE Publications b.v., Houten, 374 pp.

Bałazińska, J. & Bossowski, A., 1979. Internal geological structure of the central and western part of the North-Sudetic Synclinorium in light of new data. *Geological Quarterly*, 23: 309–322. [In Polish, with English summary.]

Berezowski, Z. & Berezowska, B., 1981. *Szczegółowa Mapa Geologiczna Sudetów, arkusz Bolesławiec 1:25 000*. Wydawnictwa Geologiczne, Warszawa. [In Polish.]

Chrząstek, A., 2002. Stratigraphy and sedimentary conditions of the Röt and Lower Muschelkalk in the North Sudetic Basin. *Acta Universitatis Wratislaviensis 2383, Prace Geologiczno-Mineralogiczne*, 73: 1–178. [In Polish, with English summary.]

Chrząstek, A. & Wojewoda, J., 2011. Mesozoic of SW Poland (North Sudetic Synclinorium). In: Żelaźniewicz, A., Wojewoda, J. & Ciężkowski, W. (eds), *Mezozoik i kenozoik Dolnego Śląska. 81 Zjazd Polskiego Towarzystwa Geologicznego.* Wydawnictwo Wind, Wrocław, pp. 1–10. [In Polish, with English summary.]

Cohen, K. M., Finney, S. C., Gibbard, P. L. & Fan, J.-X., 2013. The ICS International Chronostratigraphic Chart. *Episodes*, 36: 199–204.

Cymerman, Z., 2004. *Tectonic Map of the Sudetes and the Fore-Sudetic Block*, *1:200 000*. Państwowy Instytut Geologiczny, Warszawa.

Dadlez, R., 1998. Devonian to Cretaceous epicontinental basin in Poland: relationships between their development and structure of the crystalline crust. *Prace Państwowego Instytutu Geologicznego,* 165: 17–30. [In Polish, with English summary.]

Dadlez, R., Marek, S. & Pokorski, J. (eds), 1998. *Paleogeographical Atlas of the Epicontinental Permian and Mesozoic in Poland (1 : 2 500 000)*. Państwowy Instytut Geologiczny, Warszawa.

Dadlez, R., Marek, S., Pokorski, J. & Buła, Z., 2000. *Geological Map of Poland without Cainozoic Deposits 1:1 000 000*. Państwowy Instytut Geologiczny, Warszawa.

Drozdowski, S., Falecki, W. & Engel, W., 1978. *Dokumentacja geologiczna złoża rud miedzi „Wartowice" w kategorii C2 gm. Bolesławiec i Warta Bolesławiecka, woj. legnickie i jeleniogórskie*. Kombinat Geologiczny „Zachód" we Wrocławiu, Archiwum CAG PIG, Warszawa, 197 pp. [In Polish; Unpublished documentation.]

Durkowski, K., 2022. Record of earthquakes phenomena in a Lower-Middle Triassic sedimentary basin (North Sudetic Synclinorium - Lower Silesia, SW Poland). *Geological Quarterly*, 66: 1–18.

Durkowski, K., Sokalski, D. & Durkowska, A., 2017. The uppermost clastic succession of the lower-middle Buntsandstein as a record of continuous sedimentation during Early Triassic transgression in the Grodziec Syncline area, Sudetes. *Biuletyn Państwowego Instytutu Geologicznego*, 469: 129–154. [In Polish, with English summary.]

Dżułyński, S., 1966. Sedimentary structures resulting from convection-like patterns of motion. *Rocznik Polskiego Towarzystwa Geologicznego,* 36: 3–21. [In Polish, with English summary.]

Feist-Burkhardt, S., Götz, A. E., Szulc, J., Borkhataria, R., Geluk, M. C., Haas, J., Hornung, J., Jordan, P., Kempf, O., Michalik, J., Nawrocki, J., Reinhardt, L., Ricken, W., Röhling, H.-G., Rüffer, T., Török, Á. & Zühlke, R., 2008. Triassic. In: McCann, T. (ed.), *The Geology of Central Europe Vol. 2: Mesozoic and Cenozoic.* The Geological Society, London, pp. 749–822.

Gajewska, I., 1964. Roethian, Muschelkalk and Keuper in the western and central parts of the Fore-Sudetic Monocline. *Kwartalnik Geologiczny*, 8: 598–608. [In Polish, with English summary.]

Geluk, M. C., 2005. *Stratigraphy and Tectonics of Permo-Triassic Basins in the Netherlands and Surrounding Areas*. Ph.D. Thesis. Utrecht University, 171 pp.

Geluk, M. C. & Röhling, H.-G., 1997. High-resolution sequence stratigraphy of the Lower Triassic 'Buntsandstein' in the Netherlands and northwestern Germany. *Geologie en Mijnbouw*, 76: 227–246.

Głuszyński, A., Bobek, K. & Roman, M., 2019. *Reinterpretacja danych sejsmicznych 2D oraz model rozwoju strukturalnego w rejonie synkliny Bolesławca (synklinorium północnosudeckie)*. In: *Odtworzenie układu naprężeń i rozwoju strukturalnego synklinorium północnosudeckiego w okresie perm-kreda*. Archiwum KGHM Cuprum Sp. z o.o. – Centrum Badawczo-Rozwojowe, Wrocław, 19 pp. [In Polish; Unpublished report of the Project M/18/0007.]

Gradziński, R., Kostecka, A., Radomski, A. & Unrug, R., 1986. *Zarys sedymentologii*. Wydawnictwo Geologiczne, Warszawa, 628 pp. [In Polish.]

Heunisch, C., 1999. Die Bedeutung der Palynologie für Biostratigraphie und Fazies in der Germanischen Trias. In: Hauschke N. & Wilde V. (eds), *Trias, Eine ganz andere Welt, Mitteleuropa im frühen Erdmittelalter*. Verlag Dr. Friedrich Pfeil, München, pp. 207–220.

Hielscher, P. & Hartsch, J., 2010. 3D Modelling of the Kupferschiefer area in Poland and Germany. [Presentation on the Malta Workshop of the ProMine research project, EC 7th Frame Programme, CP-ProMine FP7-NMP-2008-LARGE-2.]

Jaglarz, P. & Rychliński, T., 2018. Solution-collapse breccias in the Upper Olenekian-Ladinian succession, Tatra Mts, Poland. *Annales Societatis Geologorum Poloniae*, 88: 303–319.

Kley, J. & Voigt, T., 2008. Late Cretaceous intraplate thrusting in central Europe: Effect of Africa-Iberia-Europe convergence not Alpine collision. *Geology,* 33: 839–842.

Kłapciński, J., 1959. The Triassic north-east of the Fore-Sudetic Swell. *Rocznik Polskiego Towarzystwa Geologicznego*, 28: 361–412. [In Polish, with English summary.]

Krumbein, W. C. & Sloss, L. L., 1963. *Stratigraphy and Sedimentation*. *Second Edition*. Freeman & Co., San Francisco, 660 pp.

Krzywiec, P., 2004. Triassic evolution of the Kłodawa salt structure: basement-controlled salt tectonics within the Mid-Polish Trough (Central Poland). *Geological Quarterly*, 48: 123–134.

Kürschner, W. M. & Herngreen, W. G. F., 2010. Triassic palynology of central and northwestern Europe: a review of palynological diversity patterns and biostratigraphic subdivisions. *Geological Society, London, Special Publication,* 334: 263–283.

Leszczyński, S., 2018. Integrated sedimentological and ichnological study of the Coniacian sedimentation in North Sudetic Basin, SW Poland. *Geological Quarterly*, 62: 767–816.

Leśniak, T., 1973. Spągowe osady retu w południowo-wschodniej części niecki bolesławieckiej. *Przegląd Geologiczny*, 12: 669–671. [In Polish.]

Leśniak, T., 1978. Profil litostratygraficzny utworów retu i wapienia muszlowego w depresji północnosudeckiej. *Geologia, Zeszyty Naukowe AGH*, 4: 6–26. [In Polish.]

Leśniak, T., 1979. Rozwój osadów retu i wapienia muszlowego w depresji północnosudeckiej na tle ich wykształcenia w Polsce południowej. *Geologia, Zeszyty Naukowe AGH*, 4: 29–43. [In Polish.]

Mastalerz, K., 1987. The Lower Permian sedimentary history of the Wolbromek Trough, SW Poland. *Symposium on Rotliegendes in Central Europe, Erfurt, May 24–30, 1987*. *Abstracts*. Academy of Sciences of the GDR, Central Institute for Physics of the Earth, Podstadm, p. 36.

Mastalerz, K., 1990. Lacustrine successions in fault-bounded basins: 1. Upper Anthracosia Shale (Lower Permian) of the North Sudetic Basin, SW Poland. *Annales Societatis Geologorum Poloniae*, 60: 75–106.

Matysik, M. & Szulc, J., 2019. Shallow-marine carbonate sedimentation in a tectonically mobile basin, the Muschelkalk (Middle Triassic) of Upper Silesia (southern Poland). *Marine and Petroleum Geology*, 107: 99–115.

Mazur, S., Aleksandrowski, P., Turniak, K., Krzemiński, L., Mastalerz, K., Górecka-Nowak, A., Kurowski, L., Krzywiec, P., Żelaźniewicz, A. & Fanning, M. C., 2010. Uplift and late orogenic deformation of the Central European Variscan belt as revealed by sediment provenance and structural record in the Carboniferous foreland basin of western Poland. *International Journal of Earth Sciences,* 99: 47–64.

Mazur, S., Scheck-Wenderoth, M. & Krzywiec, P., 2005. Different modes of the Late Cretaceous–Early Tertiary inversion in the North German and Polish basins. *International Journal of Earth Sciences*, 94: 782–798.

Menning, M. & Hendrich, A., 2017. *Stratigraphische Tabelle von Deutschland Kompakt 2017.* Deutsche Stratigraphische Kommission (DSK), Potsdam (Geoforschungszentrum), Forsch.-Inst. Senckenberg, Frankfurt a. M.

Milewicz, J., 1962. Uwagi o recie południowej części niecki północnosudeckiej. *Przegląd Geologiczny*, 7: 364–365. [In Polish.]

Milewicz, J., 1968. The geological structure of the North-Sudetic Depression. *Biuletyn Instytutu Geologicznego*, 227: 5–27. [In Polish, with English summary.]

Milewicz, J., 1976. Rotliegendes in the vicinity of the fore-sudetic block. *Kwartalnik Geologiczny*, 20: 81–95. [In Polish, with English summary.]

Milewicz, J., 1985. Proposal of a formal stratigraphic scheme for deposits infilling the North Sudetic Basin. *Przegląd Geologiczny*, 33: 385–390. [In Polish, with English summary.]

Miluk, A., Pałetko, G., Sito, Ł. & Targosz, P., 2016. *Dokumentacja z prac geofizycznych metodą sejsmiki refleksyjnej 2D.* In: *Kompleksowa obsługa geologiczna projektów Synklina Grodziecka i Konrad.* Archiwum KGHM Cuprum Sp. z o.o. – Centrum Badawczo-Rozwojowe, Wrocław, 65 pp. [In Polish; Unpublished project.]

Mroczkowski, J., 1969. Paleocurrents in the Lower Triassic deposits of the southern part of the Northsudetic Basin. *Bulletin de l'Académie Polonaise des Sciences, Série des Sciences Geologiques et Geographiques,* 17: 167–172.

Mroczkowski, J., 1972. Sedimentation of the Bunter in the North-Sudetic Basin. *Acta Geologica Polonica*, 22: 351–377. [In Polish, with English summary.]

Noetling, F., 1880. Die Entwicklung der Trias in Niederschlesien. *Zeitschrift der Deutschen Geologischen Gesellschaft*, 32: 300–349.

Orłowska-Zwolińska, T., 1983. Palynostratigraphy of the Upper part of Triassic epicontinental sediments in Poland. *Prace Instytutu Geologicznego*, 104: 1–89. [In Polish, with English summary.]

Orłowska-Zwolińska, T., 1984. Palynostratigraphy of the Buntsandstein in section of Western Poland. *Acta Palaeontologica Polonica*, 29: 161–194.

Orłowska-Zwolińska, T., 1985. Palynological zones of the Polish epicontinental Triassic. *Bulletin of the Polish Academy of Sciences, Earth Sciences*, 33: 107–119.

Ostromęcki, A., 1973. Development of the Late Palaeozoic sedimentary basins of the Kaczawa Mts. *Rocznik Polskiego Towarzystwa Geologicznego*, 43: 319–362.

Patruno, S., Kombrink, H. & Archer, S. G., 2020. Cross-border stratigraphy of the Northern, Central and Southern North Sea: a comparative tectono-stratigraphic megasequence synthesis. In: Patruno, S., Archer, S. G., Chiarella, D., Howell, J. A., Jackson, C. A.-L. & Kombrink, H. (eds), *Cross-Border Themes in Petroleum Geology I: The North Sea*. *Geological Society, London, Special Publications*, 494: 13–83.

Raczyński, P., Kurowski, L. & Mastalerz, K., 1998. Lithostratigraphy and evolution of the North Sudetic basin at the turn of the Paleozoic and Mesozoic. In: Wojewoda, J. (ed.), *Ekologiczne Aspekty Sedymentologii*. Wydawnictwo Wind, Wrocław, pp. 75–100. [In Polish, with English summary.]

Ratajczyk, M., Galica, A., Kwaśny, L., Pyra, J., Pawlak, A. & Durkowski, K., 2015. *Sprawozdanie końcowe z realizacji I i II etapu prac geologicznych na obszarze koncesyjnym „Synklina grodziecka"*. Archiwum KGHM Cuprum Sp. z o.o. – Centrum Badawczo-Rozwojowe, Wrocław, 106 pp. [In Polish; Unpublished documentation.]

Schlumberger, 1974. *Log Interpretation. Volume II – Applications*. Edition Schumberger Ltd., 116 pp.

Scupin, H., 1902. Die Gliederung der Schichten in der Goldberger Mulde. *Zeitschrift der Deutschen Geologischen Gesellschaft*, 54: 99–108.

Scupin, H., 1913. Die Löwenberger Kreide und ihre Fauna. *Palaeontographica – Supplementbände*, 6: 1–275.

Scupin, H., 1932. Die oberschlesische Buntsandsteinfrage und die epeirogenen Kippungsbewegungen der Röttransgression in Ostdeutschland. *Zeitschrift der Deutschen Geologischen Gesellschaft,* 84: 543–554.

Senkowiczowa, H., 1965. Facial development of the Roethian deposits in the area of southern Poland. *Geological Quarterly*, 9: 241–260. [In Polish, with English summary.]

Sokołowski, J., 1967. Geological and structural characteristics of the Fore-Sudetic area. *Geologia Sudetica*, 3: 297–357. [In Polish, with English summary.]

Solecki, A. T., 2011. Structural evolution of the epi-Variscan platform cover in the North Sudetic Synclinorium. In: Żelaźniewicz, A., Wojewoda, J. & Ciężkowski, W. (eds), *Mezozoik i Kenozoik Dolnego Śląska. 81 Zjazd Polskiego Towarzystwa Geologicznego.* Wydawnictwo Wind, Wrocław, pp. 19–36. [In Polish, with English summary.]

Szulc, J., 2000. Middle Triassic evolution of the northern peri-Tethys area as influenced by early opening of the Tethys Ocean. *Annales Societatis Geologorum Poloniae*, 70: 1–48

Szulc, J., Becker, A. & Mader, A., 2015. Perm i trias – nowe otwarcie w historii Gór Świętokrzyskich. In: Skompski, S. (ed.), *Ekstensja i inwersja powaryscyjskich basenów sedymentacyjnych. 84 Zjazd Naukowy Polskiego Towarzystwa Geologicznego, Chęciny, 9–11 września 2015 r.* Państwowy Instytut Geologiczny, Warszawa, pp. 11–27. [In Polish.]

Szyperko-Śliwczyńska, A., 1980. Lithostratigraphy of the Buntsandstein of Poland and project of its systematization. *Geological Quarterly*, 24: 275–298. [In Polish, with English summary.]

Szyperko-Teller, A., 1997. Trias dolny (pstry piaskowiec). Litostratygrafia i litofacje. Formalne i nieformalne jednostki litostratygraficzne. In: Marek, S. & Pajchlowa, M. (eds), *Epikontynentalny perm i mezozoik w Polsce. Prace Państwowego Instytutu Geologicznego*, 153: 112–117. [In Polish.]

Śliwiński, W., Raczyński, P. & Wojewoda, J., 2003. Sedymentacja utworów epiwaryscyjskiej pokrywy osadowej w basenie północnosudeckim. In: Ciężkowski, W., Wojewoda, J. & Żelaźniewicz, A. (eds), *Przewodnik do wycieczek 74 Zjazdu Polskiego Towarzystwa Geologicznego.* Wydawnictwo Wind, Wrocław, pp. 10–17. [In Polish.]

Tokarski, A., 1965. Stratigraphy of the salinary of the Fore-Sudetic Monocline. *Acta Geologica Polonica*, 15: 105–129. [In Polish, with English summary.]

Visscher, H., 1974. The impact of palynology on Permian and Triassic stratigraphy in western Europe. *Review of Palaeobotany and Palynology*, 17: 5–19.

Visscher, H., 1980. Aspects of a palynological characterization of the Late Permian and Early Triassic "standard" units of chronostratigraphical classification in Europe. In: *Proceedings 4th International Palynological Conference, Lucknow 1976–77*, 2: 238–244.

Watycha, L., 1951. Geologia niecki grodzieckiej na Dolnym Śląsku, Księga pamiątkowa ku czci Prof. K. Bohdanowicza. *Prace Państwowego Instytutu Geologicznego*, 7: 199–215. [In Polish.]

Wojewoda, J. & Mastalerz, K., 1989. Climate evolution, allocyclic and autocyclic sedimentation on the side of the Upper Carboniferous and Permian continental sediments in the Sudetes. *Przegląd Geologiczny*, 37: 173–180. [In Polish, with English summary.]

Ziegler, P. A., 1982. Triassic rifts and facies patterns in Western and Central Europe. *Geologische Rundschau*, 71: 747–772.

Appendix 1

Occurrence of palynomorphs in analysed samples.

Borehole/Outcrop	W-I/1			W-I/3W		W-III/2		W-III/4W			W-V/3		W-V/6W			W-VII/4W			W-VII/6			W-IX/6W			W-XI/6W				Rac. 1	Jerz. 1. t.	Jerz. 1. b.
Palynomorphs \ Depth [m]	127.5	200.0	207.0	33.0	62.5	85.5	110.0	382.0	411.0	418.0	65.0	97.5	572.0	572.5	574.5	297.0	333.5	360.5	444.0	448.0	525.0	250.0	296.0	327.0	61.5	91.5	153.0	157.0			
SPORES																															
Calamospora tener (Leschik) de Jersey				x				x		x							x				x		x								x
Calamospora sp.			x	x				x	x									x	x			x	x					x		x	
Psilatriletes triassicus Visscher				x	x				x					x	x		x		x		x		x				x				x
Punctatisporites triassicus Schulz	x	x	x	x	x		x		x	x	x	x		x	x		x	x	x	x	x			x	x		x				x
Punctatisporites sp.		x	x		x				x	x		x		x			x		x		x							x			
Cyclotrites microgranifer Mädler		x	x	x					x		x	x		x	x			x			x		x	x	x						x
Cyclotrites oligogranifer Mädler			x		x			x				x					x		x		x						x	x			
Cyclotrites triassicus Mädler		x	x	x	x			x		x	x	x		x	x	x		x	x	x	x		x	x	x		x	x		x	x
Cyclotriletes sp.		x	x				x	x			x			x	x	x					x			x	x				x	x	
Apiculatisporites plicatus Visscher		x										x					x														
Apiculatisporites sp.											x													x							
Anapiculatisporites sp.		x		x										x																	x
Verrucosisporites aff. *jenensis* Visscher				x																											
Verrucosisporites morulae Klaus				x						x		x		x	x		x	x	x				x				x				
Verrucosisporites pseudomorulae Visscher	x		x	x							x	x					x		x		x	x								x	x
Verrucosisporites thuryngiacus Mädler		x	x	x						x	x	x		x			x	x	x		x	x	x				x				
Verrucosisporites sp.	x	x	x	x	x		x			x	x	x		x			x	x	x		x		x	x			x			x	x
Guttatisporites elegans Visscher			x	x					x					x							x	x		x			x			x	
Guttatisporites guttatus Visscher		x		x					x					x				x	x					x			x				
Guttatisporites microechinatus Visscher		x	x	x	x		x	x	x	x	x	x		x	x		x	x	x					x				x		x	
Lapposisporites lapposus Visscher				x						x	x			x			x						x								
Lapposisporites villosus Visscher				x	x						x			x	x								x				x				
Lapposisporites sp.				x	x					x	x	x		x			x		x				x							x	
Baculatisporites verus Orłowska -Zwolińska				x					x															x							x
Baculatisporites sp.		x						x		x							x			x			x	x							x
Densoisporites nejburgii (Schulz) Balme				x	x						x						x	x			x		x	x			x	x			
Densoisporites playfordii (Balme) Dettmann			x														x				x		x				x				
Densoisporites sp.			x	x	x					x	x							x			x		x	x		x					
Paralundbladispora sp.					x													x						x			x				
Kraeuselisporites hystrix Visscher			x						x					x			x						x								
Kraeuselisporites ulllrichi Reinchardt et Schmitz			x								x	x					x	x	x			x					x				
Kraeuselisporites sp.			x	x	x		x		x	x	x	x		x	x	x	x	x	x		x	x	x				x	x			x
Perotrilites minor Antonescu et Taugordeau-Lanz	x	x																							x						
aff. *Perotriletes* sp.				x																					x						
Concentricisporites nevesi Antonescu									x									x				x		x							x
Aratrisporites granulatus (Klaus) Playford et Dettmann		x	x	x							x						x	x						x				x			
Aratrisporites flexibilis Playford et Dettmann		x	x		x																										

Borehole/Outcrop	W-I/1			W-I/3W		W-III/2		W-III/4W			W-V/3		W-V/6W			W-VII/4W			W-VII/6			W-IX/6W			W-XI/6W				Rac. 1	Jerz. 1. t.	Jerz. 1. b.
Depth [m] / Palynomorphs	127.5	200.0	207.0	33.0	62.5	85.5	110.0	382.0	411.0	418.0	65.0	97.5	572.0	572.5	574.5	297.0	333.5	360.5	444.0	448.0	525.0	250.0	296.0	327.0	61.5	91.5	153.0	157.0			
Aratrisporites tenuispinosus Playford			x				x											x													
Aratrisporites sp.			x		x			x		x							x	x					x	x				x			
POLLEN GRAINS																															
Accinctisporites sp.			x	x	x					x	x			x				x	x	x		x	x	x			x			x	
Ellipsovelatisporites rugulatus Orłowska-Zwolińska					x						x	x										x									
Nuskoisporites dulhuntyi Potonié ekt Klaus					x																										
Nuskoisporites klausii Grebe					x																										
Nuskoisporites inopinatus Visscher				x	x									x			x													x	
Stellapollenites thiergartii (Mädler) Clement-Westerhof et al. emend. Brugman	x	x	x	x	x		x		x	x	x	x				x	x		x			x	x	x			x	x		x	
Protohaploxypinus jacobii (Jansonoius) Hart									x	x		x					x	x					x								
Protohaploxypinus pennatulus Hart																	x	x	x				x				x				
Protohaploxypinus samoilovichii (Jansonius) Hart				x				x	x	x		x					x	x	x		x		x				x				
Protohaploxypinus sp.			x	x	x		x	x	x	x	x	x				x	x	x		x	x		x	x		x		x	x	x	
Striatoabietites aytugii Visscher				x								x			x		x	x	x				x	x			x				
Striatoabietites balmei Klaus		x		x				x	x	x	x				x	x	x	x					x	x			x				
Striatoabietites sp.	x	x			x							x		x	x			x				x		x			x			x	x
Distriatites sp.										x																					
Staurosaccites sp.				x						x		x									x			x							
Lueckisporites virkkiae Potonié et Klaus			x	x			x									x	x	x					x	x			x	x			
Lunatisporites albertae (Jansonius) Fijałkowska			x					x	x	x	x	x		x	x			x	x		x		x				x	x			
Lunatisporites gracilis (Jansonius) Fijałkowska			x	x				x	x				x				x	x	x					x			x	x			
Lunatisporites microsaccatus (Jansonius) Fijałkowska									x								x	x			x						x				
Lunatisporites multiplex (Visscher) Scheuring			x	x	x			x				x		x			x	x				x	x	x			x				
Lunatisporites novaiulensis (Leschik) Scheuring			x	x	x		x	x	x	x	x	x		x			x	x			x	x	x	x			x		x		x
Lunatisporites puntii Visscher		x	x	x							x	x			x			x	x					x							x
Lunatisporites transversundatus (Jansonius) Fijałkowska								x	x		x						x	x			x										
Lunatispsorites sp.			x	x	x		x	x		x	x		x	x	x	x	x	x		x	x	x	x	x				x	x	x	x
aff. *Ovalipollis* sp.																	x						x						x		
Paravesicaspora planderovae Visscher		x								x																					
Paravesicaspora sp.	x									x													x								
Klausipollenites decipiens Jansonius											x							x													
Klausipollenites staplinii Jansonius	x							x			x			x				x	x				x	x			x				
Klausipollenites sp.	x		x		x		x	x			x	x		x		x	x	x	x		x	x	x	x		x		x			
Falcisporites snopkovae Visscher																															
Falcisporites sp.										x	x						x				x	x	x						x		
Brachysaccus ovalis Mädler		x	x		x			x	x	x	x	x	x	x	x	x	x	x	x		x	x	x	x		x	x	x	x	x	
Chordasporites voltziaformis Visscher		x															x														
Colpectopollis ellipsoideus Visscher			x		x				x									x			x							x			
Minutosaccus (Protodiploxypinus) sp.		x	x																				x				x				
Microcahryidites doubingeri Klaus		x	x	x			x	x				x					x		x	x	x	x	x	x	x		x	x	x		x

Borehole/Outcrop	W-I/1			W-I/3W		W-III/2		W-III/4W			W-V/3		W-V/6W			W-VII/4W			W-VII/6			W-IX/6W			W-XI/6W				Rac. 1	Jerz. 1. t.	Jerz. 1. b.
Palynomorphs \ Depth [m]	127.5	200.0	207.0	33.0	62.5	85.5	110.0	382.0	411.0	418.0	65.0	97.5	572.0	572.5	574.5	297.0	333.5	360.5	444.0	448.0	525.0	250.0	296.0	327.0	61.5	91.5	153.0	157.0				
Microcahryidites fastidiosus (Jansonius) Klaus			x	x			x	x	x	x			x				x	x	x	x	x	x		x			x		x	x	x
Microcahryidites sittleri Klaus		x	x	x	x		x	x	x								x		x	x		x		x	x		x			x	x
Microcahryidites sp.	x	x		x							x					x	x	x		x	x	x	x			x	x		x	x	x
Voltziaceaesporites heteromorpha Klaus		x	x	x	x		x	x	x	x	x	x	x	x	x		x	x	x		x	x	x	x				x	x		x
Alisporites grauvogeli Klaus		x		x	x																	x	x								
Alisporites toralis (Leschik) Clarke									x					x																	
Alispsorites sp.		x		x	x				x	x	x	x		x	x	x	x	x	x		x	x	x	x			x	x		x	x
Platysaccus leschiki Hart												x					x							x			x				
Platysaccus papilionis Potonié et Klaus				x														x													x
Platysaccus sp.			x							x						x	x				x	x	x	x				x		x	x
Illinites chitonoides Klaus		x	x	x			x	x	x		x		x		x	x	x	x	x	x	x	x		x		x	x				
Jugasporites delasaucei (Potonié et Klaus) Leschik				x																											
*Jugasporites paradelasaucei K*laus				x																			x								
Jugasporites sp.							x										x														
Angustisulcites gorpii Vissscher	x		x	x	x				x		x	x		x	x		x	x	x	x	x	x	x	x			x	x	x	x	x
Angustisulcite grandis (Freudenthal) Visscher			x	x			x		x	x		x		x			x	x		x	x		x				x	x		x
Angustisulcites klausi Freudenthal		x	x	x	x		x	x	x	x	x	x	x	x	x	x		x	x	x	x	x	x	x	x		x			x	x
Angustisulcites sp.	x	x	x	x	x			x	x	x	x		x				x				x	x	x			x	x	x	x	x	x
Triadispora aurea Klaus																x				x											
Triadispora crassa Klaus	x	x	x	x	x		x	x	x	x	x	x	x	x			x	x	x	x	x	x	x	x	x	x		x	x	x	x
Triadispora plicata Klaus	x		x	x			x	x	x		x	x					x	x	x	x							x		x		
Triadispora stabilis Scheuring				x	x						x					x	x	x	x	x	x	x	x	x			x				
Triadispora suspecta Scheuring		x	x	x			x	x	x		x	x		x	x		x	x			x	x		x			x				
Triadispora sp.	x		x	x	x		x	x	x		x	x	x				x	x	x	x	x	x	x	x		x		x		x	x
Cycadopites coxii Visscher		x	x								x			x	x		x	x					x					x	x		
Cycadopites follicularis Wilson et Webster		x		x							x						x		x												
MICROPHYTOPLANKTON																															
ACRITARCHS																															
Baltisphaeridium sp.				x																					x						
Micrhystridium inconspicuum (Deflandre) Deflandre				x																											
Micrhystridium sp.				x																					x						
Veryhachium irregulare Jekhowsky											x																				
Veryhachium trispinosum Eisenack											x								x												
Veryhachium sp.											x								x						x						
PRASINOPHYTES																															
Leiosphaeridia sp.		x																													
Tasmanites sp.	x	x																													
Crassosphaera sp.	x	x																													
Dictyotidium sp.		x																													
Reduviasporonites catenulatus Wilson		x	x																					x							
Schizosporis sp.	x	x	x													x											x				

Abbreviations: Rac. – Raciborowice; Jerz. – Jerzmanice l; b. – base; t. – top.